Biomechanics and Modeling in Mechanobiology (2023) 22:785–808
https://doi.org/10.1007/s10237-022-01681-3

ORIGINAL PAPER

Biomechanical activation of blood platelets via adhesion to von Willebrand factor studied with mesoscopic simulations

Aleksey V. Belyaev[1] · **Yulia K. Kushchenko**[1]

Received: 22 September 2022 / Accepted: 22 December 2022 / Published online: 10 January 2023

Abstract
Platelet adhesion and activation are essential initial processes of arterial and microvascular hemostasis, where high hydrodynamic forces from the bloodflow impede coagulation. The process relies on von Willebrand factor (VWF)—a linear multimeric protein of blood plasma plays a pivotal role in mechanochemical regulation of shear-induced platelet aggregation (SIPA). Adhesive interactions between VWF and glycoprotein receptors GPIb are crucial for platelet recruitment under high shear stress in fluid. Recent advances in experimental studies revealed that mechanical tension on the extracellular part of GPIb may trigger a cascade of biochemical reactions in platelets leading to activation of integrins $\alpha_{\mathrm{IIb}}\beta_3$ (also known as GPIIb/IIIa) and strengthening of the adhesion. The present paper is aimed at investigation of this process by three-dimensional computer simulations of platelet adhesion to surface-grafted VWF multimers in pressure-driven flow of platelet-rich plasma. The simulations demonstrate that GPIb-mediated mechanotransduction is a feasible way of platelet activation and stabilization of platelet aggregates under high shear stress. Quantitative understanding of mechanochemical processes involved in SIPA would potentially promote the discovery of new anti-platelet medication and the development of multiscale numerical models of platelet thrombosis and hemostasis.

Keywords Platelet adhesion · von Willebrand factor · Shear-induced activation · Numerical simulations

1 Introduction

Adhesion, aggregation and activation of blood platelets are essential stages of primary hemostasis and thrombosis in arteries and microvasculature, where intensive bloodflow and shear stress inhibit fibrin polymerization (Kuijpers et al. (2009); Stalker et al. (2013); Furie and Furie (2005)). Several studies demonstrated that thrombogenesis depends on local hemodynamics (Jackson et al. (2009); Westein et al. (2013); Nesbitt et al. (2009)), adhesion between receptor proteins located on platelet membranes with their ligands dissolved in blood plasma (Jackson et al. (2009); Maxwell et al. (2007); Springer (2014); Clemetson and Clemetson (2014); Andrews et al. (2007); Plow and Pesho (2007)), mechanosensitive proteins (Schneider et al. (2007); Santamaría et al. (2015)) and mechanotransduction (Hansen et al. (2018)).

Von Willebrand factor (VWF) is a complex multimeric plasma protein that plays a central role in initial stages of platelet hemostasis (Maxwell et al. (2007)), arterial and microvascular thrombosis (Springer (2014); Okhota et al. (2020)) and shear-induced platelet aggregation (SIPA) (Schneider et al. (2007); Jackson et al. (2009); Rana et al. (2019); Liu et al. (2021); O'Brien (1990); Shankaran et al. (2003); Liu et al. (2022)). This protein is a ligand to platelet glycoprotein receptors GPIb and integrins $\alpha_{\mathrm{IIb}}\beta_3$ (also known as GPIIb/IIIa)—principal adhesive proteins of platelets (Kim et al. (2010); Clemetson and Clemetson (2014); Andrews et al. (2007); Plow and Pesho (2007)). It also carries and protects the clotting factor VIII from proteolysis (Dong et al. (2019)). The linear, chain-like concatemer structure of VWF is meant to provide mechanosensing qualities in blood circulation system (Fowler et al. (1985); Springer (2014)). A multimer dissolved in blood plasma adopts a compact "coil" conformation under low to moderate hydrodynamic forces, and extends into long "strings" when shear or elongational stresses in blood exceed a certain threshold (Schneider et al. (2007); Ruggeri (2001)). Inflamed endothelium can secrete and anchor (ultra-)long VWF strings causing prothrombotic

✉ Aleksey V. Belyaev
aleksey_belyaev@yahoo.com

[1] Faculty of Physics, M.V. Lomonosov Moscow State University, 1-2 Leninskiye Gory, Moscow, Russia 119991

conditions (Ceunynck et al. (2013)), which may be one of the factors of thrombo-inflammatory complications of COVID-19 (Choudhary et al. (2021)).

It has been shown experimentally that healthy VWF can effectively bind platelets only as a result of force-induced conformational change in the dimeric subunits of this protein (Fu et al. (2017); Jiang et al. (2019)). A mechanical stimulus of sufficient amplitude can cause several sequential changes in conformation of the VWF protein, alter the molecular environment of its principal platelet-binding domain VWF-A1, and cease the autoinhibitory effect that arises from neighboring domains and unstructured linkers (Aponte-Santamaria et al. (2015); Arce et al. (2021); Zhao et al. (2022)). The typical tension force required for activation of VWF monomers was estimated as 20–35 pN by Fu et al. (2017). Various mutations cause abnormal VWF-GPIb binding leading to unwanted thrombotic or bleeding effects (Yago et al. (2008); Colace and Diamond (2013)). It was also shown that VWF multimers attached to the surface of a blood vessel or the wall of a flow chamber are more easily uncoiled and activated, as compared to the free-flowing proteins (Belyaev (2018); Schwarzl and Netz (2018); Kushchenko and Belyaev (2020)), and that length of these multimers is an important parameter for both VWF activation (Kushchenko and Belyaev (2020); Wang et al. (2019)) and platelet binding (Belyaev (2018); Furlan (1996)).

Glycoprotein Ib (GPIb) receptors are abundant on the outer membrane of circulating platelets in the form of the GPIb-IX-V complex. Its adhesive chain GPIbα binds to A1 domain of VWF and provides initial platelet adhesion to vascular injury (e.g., exposed sub-endothelial collagen), ruptured atherosclerotic plaque or inflamed endothelium (Rusu and Minshall (2018); Gardiner and Andrews (2014); Springer (2014)). Numerous efforts of scientists and clinicians are aimed at deeper understanding of GPIb-VWF interactions, since it may help in the treatment of hereditary bleeding disorders (Lanza (2006); Swami and Kaur (2016); Hovinga et al. (2017)). Several studies report that defective binding of mutant GPIb and/or VWF variants may lead to significant alterations of platelet adhesion as function of shear stress (Yago et al. (2008); Konstantopoulos et al. (1997); Kumar et al. (2003)). Interestingly, these mutant variants may not only decrease platelet affinity to VWF, but often increase it, as follows from the measured bond lifetime under low and intermediate shear stress (Yago et al. (2008); Kumar et al. (2003)), suggesting that the unstretched (inactive) VWF subunits may also be adhesive to platelets in cases of particular dysfunctions. Although GPIb is not the only platelet adhesion receptor responsible for growth, biomechanical properties and integrity of arterial thrombi, it is the only one that can effectively bind platelets in fast blood flows and high shear stress (Ruggeri et al. (2006); Savage and Ruggeri (2007); Jackson et al. (2009); Nesbitt et al. (2009)). GPIb-VWF bonds can independently capture and hold the discoid platelets from the blood stream, bearing a high mechanical load (Nesbitt et al. (2009)). However, several works underline transient and reversible character of this shear-induced GPIb-dependent platelet aggregation, unless platelet *activation* takes place (Savage et al. (1996); Goto et al. (1995); Westein et al. (2013)).

Adhered platelets can get activated by different cellular signaling pathways, initiated by receptor-ligand interactions and resulting in activation of $\alpha_{\mathrm{IIb}}\beta_3$ integrins on platelet membranes. This leads to formation of stable platelet aggregates due to binding between $\alpha_{\mathrm{IIb}}\beta_3$ and VWF (Chow et al. (1992); Konstantopoulos et al. (1997)) or fibrinogen (Coller and Shattil (2008)). Unlike the GPIb receptor, the integrin $\alpha_{\mathrm{IIb}}\beta_3$ requires "activation" via a conformational transition between the bent (inactive, low affinity) and the extended (active, high-affinity) states (Nguyen et al. (2016); Mitchell et al. (2007); Chen et al. (2019)). An intermediate state of $\alpha_{\mathrm{IIb}}\beta_3$ activation was recently reported in the literature, Chen et al. (2019), being hypothetically associated with the biomechanical pathway of platelet activation.

The biochemical pathway of platelet activation mediated by soluble agonists, such as adenosine diphosphate (ADP), thrombin and thromboxane A2, requires from tens of seconds to minutes (Poole and Watson (1995); Würtz et al. (2013); Obydennyy et al. (2016)), however, it is expected that in vivo activation of $\alpha_{\mathrm{IIb}}\beta_3$ should take $\approx 0.1 - 0.2$ s (Born and Richardson (1980); Richardson (1973)). The biomechanical pathway is another possibility for signaling in platelets (Zhang et al. (2019, 2015); Deng et al. (2016); Nesbitt et al. (2003)). The importance of GPIb receptors for $\alpha_{\mathrm{IIb}}\beta_3$ activation has remained controversial (Shankaran et al. (2003); Dayananda et al. (2010); Ozaki et al. (2005); Ruggeri et al. (2006); Savage et al. (1996); Goto et al. (1995)) until recent experimental studies of a juxtamembrane mechanosensitive domain (MSD) of the GPIb-IX-V complex by Zhang et al. (2019, 2015); Ju et al. (2016) suggested a novel mechanism of platelet mechanosensing, enlightening the details of the mechanical signal processing by adhering platelets. Tension forces 10–15 pN on GPIb receptors result in unfolding of MSD, transducing a mechanical signal into calcium oscillations in the cytosol of platelets, thus activating $\alpha_{\mathrm{IIb}}\beta_3$ receptors (Ju et al. (2016)) and stabilizing the aggregate (Shankaran et al. (2003); Nesbitt et al. (2009); Chow et al. (1992)). It was also found that mechanotransduction through GPIb-IX-V can activate platelet $\alpha_{\mathrm{IIb}}\beta_3$ receptors independently of other platelet receptors (Kasirer-Friede et al. (2004); Ozaki et al. (2005)). It is intriguing to determine the precise contribution of GPIb-mediated platelet adhesion and MSD unfolding to shear-induced platelet aggregation in various hemodynamic conditions.

Growing importance of modern computational methods in studies of thrombosis and hemostasis is supported

by recent advances in protein and biopolymer dynamics simulations (Ahlrichs and Dünweg (1999); Kabedev and Lobaskin (2018); Lopez and Lobaskin (2015); Rack et al. (2017); Sterpone et al. (2018); Alexander-Katz and Netz (2008); Schneider et al. (2007); Dong et al. (2019); Kushchenko and Belyaev (2020); Belyaev (2021); Languin-Cattoën et al. (2021)), cytoskeleton and intracellular mechanics (Fedosov et al. (2010); Pothapragada et al. (2015)), hemodynamic simulations at the level of individual cells (Pivkin and Karniadakis (2008); Fedosov et al. (2014); Mountrakis et al. (2015); Mody and King (2008a, 2008b); van Rooij et al. (2019); Spann et al. (2016); Belyaev (2018); Dupin et al. (2007); Bušík and Cimrák (2017); Cimrák et al. (2014, 2012)), coarse-grained and hybrid simulations (Yazdani et al. (2017); Tosenberger et al. (2016); Pivkin et al. (2006); Kaneva et al. (2021)), continuum modeling (Bouchnita and Volpert (2019); Fogelson et al. (2012); Belyaev et al. (2015); Wu et al. (2017)), and multiscale approaches (Bouchnita and Volpert (2019); Belyaev et al. (2018); Fedosov and Karniadakis (2009)). Recent examples of coarse-grained computer simulations of shear-induced platelet aggregation by Liu et al. (2022, 2021) demonstrate the capability of *in silico* approaches for the analysis of platelet hemostasis and thrombosis. However, in these works the platelets were represented by solid spherical particles, the simulations considered initial 10 ms, and the possibility of mechanical activation of $\alpha_{\mathrm{IIb}}\beta_3$ receptors was not included. The present paper makes a further step by increasing the time interval to at least 100 ms, considering realistic platelet shape and their mechanical motion, quantifying the force on GPIb receptors and investigating the possibility of biomechanical integrin activation. We report a computational study of platelet adhesion to surface-grafted VWF multimers in a pressure-driven flow of a viscous fluid. By using a hybrid particle-continuum model we investigate the feasibility of the biomechanical GPIb-mediated platelet activation in a wide range of hydrodynamic conditions. The proposed model resolves a realistic oblate shape of the blood platelets, the details of platelet motion in the flow of a viscous fluid, explicitly treats VWF multimers and platelet adhesion receptors, accounts for the biomechanical activation of VWF multimers and the force-induced triggering of GPIb mechanosensitive domain. Our main goal is to link the fluid dynamics conditions with the probability of platelet activation due to mechanical forces acting on GPIb receptors. We also strive to identify among the entire set of parameters of the system the most important ones for the shear-induced platelet adhesion and aggregation. The paper is organized as follows. Firstly, in the Methods section we describe the computational model used in the presented work. Secondly, in the Results section the main computational findings are presented, including the validation of the model, the quantification of the tension force on GPIb receptors in the simulations in different hydrodynamic conditions, the investigations of the effects of GPIb-VWF binding affinity and VWF activation on the adhesion of modeled platelets, and possible consequences of $\alpha_{\mathrm{IIb}}\beta_3$ activation for stabilization of the platelet aggregates under high shear. Then, in the Discussion section, we discuss the outcomes of our theoretical findings for general understanding of platelet thrombosis and hemostasis. Finally, we conclude in the Conclusion section.

2 Methods

The present paper studies platelet adhesion to surface-immobilized VWF multimers subjected to a pressure-driven flow of a viscous fluid by means of coarse-grained computer simulations. The numerical method is based on a combination of Lattice Boltzmann (LB) method (Succi (2001)) with Lagrangian particle dynamics (LPD) (Dünweg and Ladd (2009)). We developed a hybrid continuum-particle model on top of the ESPResSo open-source software (ver.3.4) (Limbach et al. (2006); Arnold et al. (2013)) with several modifications of the original code, including individual friction parameter for each type of particles and force-dependent activation of VWF monomers (Belyaev (2018, 2018); Kushchenko and Belyaev (2020)). The present model is an extension of our previous works, and some new features have been introduced since then. Mainly, for the purposes of the research, we implemented tracking of platelet adhesion receptors as Lagrangian particles and force-dependent activation of platelets with either deterministic or stochastic kinetics, as described further in this section.

The model consists of three principal components: viscous fluid (blood plasma or buffer liquid), blood cells (platelets) and the von Willebrand factor (VWF) multimers (linear polymers). The following scales for length, force and time were used in the model: $[L] = 10^{-6}\ m$, $[F] = 10^{-9}\ N$, $[t] = 10^{-4}\ s$. All physical values were non-dimensionalized according to these units. The system was placed in a rectangular simulation box $b_x \times b_y \times b_z$ filled with a viscous continuum fluid. Two parallel-plane no-slip boundaries (impenetrable for fluid and repulsive to particles) were introduced at $z = 0$ and $z = b_z$, while in x- and y-directions the periodic boundary conditions were set. The VWF multimers and the platelets were implemented as deformable objects consisting of Lagrangian particles interacting with the fluid by the two-way viscous coupling.

2.1 Fluid model

Continuum representation was used for modeling the hydrodynamics of the blood plasma, implemented via the Lattice Boltzmann method (LBM)—a fast solver for hydrodynamic equations, that inherits from lattice gas

automata simulations, see Succi (2001). This method rests upon the Boltzmann's kinetic equation that describes spatial–temporal changes of a one-particle distribution function $f(\mathbf{x}, \mathbf{u}, t)$:

$$\frac{\partial f}{\partial t} + \mathbf{u} \cdot \frac{\partial f}{\partial \mathbf{x}} + \frac{\mathbf{F}}{m} \cdot \frac{\partial f}{\partial \mathbf{u}} = \left(\frac{\partial f}{\partial t} \right)_{\text{coll}}, \tag{1}$$

where the term in the right-hand side is the collision integral that depends on velocities of the collided particles before and after the collision.

The D3Q19 scheme for LB was used in this work, according to which a 3D-periodic cubic lattice with a period $\Delta x = [L]$ together with 19 elementary velocity vectors $\mathbf{c}_i$ allow for the phase-space discretized form of the distribution function $f_i(\mathbf{x}, t)$, and the discrete version of Boltzmann kinetic equation reads:

$$f_i(\mathbf{x} + \mathbf{c}_i \Delta t, t + \Delta t) = f_i(\mathbf{x}, t) - F_i + \Omega_i(\mathbf{x}, t) + \chi_i, \tag{2}$$

here $f_i(\mathbf{x}, t) \equiv f(\mathbf{x}, \mathbf{c}_i, t)$ is the discrete distribution function at the lattice node $\mathbf{x}$ at the time t along the i-th elementary velocity vector $\mathbf{c}_i$, χ_i is the noise term that was chosen according to fluctuation–dissipation theorem (Adhikari et al. (2005); Dünweg and Ladd (2009); Ladd (1994); Kushchenko and Belyaev (2020)), F_i is the additional contribution due to external body forces on the fluid, and $\Omega_i(\mathbf{x}, t)$ is the collision operator (Ladd and Verberg (2001)). The collision operator $\Omega_i(\mathbf{x}, t)$ in Bhatnagar–Gross–Krook form with a single relaxation time τ was used, so that rheology of the modeled blood plasma corresponded to a viscous incompressible fluid (Succi (2001); Reasor et al. (2012); Mountrakis et al. (2015); Chen and Doolen (1998)):

$$\Omega_i(\mathbf{x}, t) = -\frac{1}{\tau} \left[f_i(\mathbf{x}, t) - f_i^{\text{eq}}(\mathbf{x}, t) \right]. \tag{3}$$

The equilibrium distribution function $f_i^{\text{eq}}(\mathbf{x}, t)$ is obtained from the series expansion of Maxwell–Boltzmann distribution for small velocities (Succi (2001); Chen and Doolen (1998)). For setting up the no-slip hydrodynamic boundaries the "link bounce back" method has been used (Dünweg and Ladd (2009)). Consequent iterations of Eq. (2) result in a temporal evolution of $f_i(\mathbf{x}, t)$, from which the observable quantities, such as fluid velocity $\mathbf{v}_{\text{fl}}$ and density ρ, are deduced (Succi (2001); Ladd and Verberg (2001)).

The model allows for simulations of platelet adhesion either in the plane shear (Couette) or in the pressure-driven (Poiseuille) flow of blood plasma, and in this work we focus on the latter case, which is typical for microfluidic devices with syringe pumping. The pressure drop across the x-coordinate in the simulation box was established by applying to the fluid a homogeneous external force density $(|\nabla p|, 0, 0)$, see Ladd and Verberg (2001).

2.2 VWF multimer model

Linear VWF multimers were represented by the "beads-and-springs" free-jointed model, implemented and validated earlier (Belyaev (2018, 2018); Kushchenko and Belyaev (2020)). Each VWF was grafted to the bottom plane wall by one of its terminus, leaving the other one free. Finitely extensible nonlinear elastic (FENE) potential was used to describe bonded interactions between the VWF beads belonging to the same multimer:

$$U_{\text{FENE}} = -\frac{1}{2} \kappa_{\text{VWF}} (\Delta r_{\max})^2 \ln \left[1 - \left(\frac{r - r_0}{\Delta r_{\max}} \right)^2 \right], \tag{4}$$

with $r_0 = 2a$, monomer radius $a = 0.05$ μm. Two other parameters—the stiffness of the chain $\kappa_{\text{VWF}} = 0.065$ mN/m and the maximal extension of a bond $\Delta r_{\max} = 0.3$ μm— were obtained by fitting the experimental data from Müller et al. (2016). The tension-induced activation of VWF monomers was implemented using a phenomenological force-dependent approach following published experimental data by Fu et al. (2017); Aponte-Santamaria et al. (2015).

Switching between the affinity of VWF-A1 domain and GPIb receptors is reported to happen in a threshold-like manner, thus if the force on an inactive VWF bead in the simulations exceeds the critical value ($F > F_{\text{actVWF}}$), then this bead is considered as activated. The activation status only changes the interaction energy between VWF bead and GPIb-particles. The critical value F_{actVWF} reported in experimental data is in the range 10–35 pN, see Fu et al. (2017); Aponte-Santamaria et al. (2015), with a plateau at 35 pN and the mid-point at 20 pN. On the other hand, mutation of VWF domains may cause alterations in the protein's resilience and ability to bind GPIb receptors, therefore, this parameter was subjected to change in our simulations within the mentioned range. Deactivation of VWF monomers was implemented, in contrast, using a geometrical criterion: if the distance r between two adjacent activated VWF beads is less than $r_0 + \delta r_{\text{inact}}$, then these VWF monomers are considered as normal (inactive) low-affinity beads, due to autoinhibitory mechanism reported in the literature by Aponte-Santamaria et al. (2015). For the present simulations $\delta r_{\text{inact}} = 0.05$ μm. Behind such "asymmetric" choice of activation conditions there stands a biophysical (molecular) background, the autoinhibition of VWF is mediated by force-dependent interdomain interactions and the VWF-A1 domain shading by neighboring VWF domains, which implies that a certain force is required to overcome the interdomain adhesive forces, yet the reverse process mostly depends of the distance between the adhesive sites of VWF-A1 domain and its molecular surroundings.

2.3 Platelet model

The platelets are represented by a triangular mesh of Lagrangian particles immersed in the fluid with a viscous Stokes-like coupling between the LB fluid and the particles (Cimrák et al. (2012, 2014); Bušík and Cimrák (2017); Belyaev (2018, 2017, 2019)). The mesh for each platelet in our simulations consisted of 102 surface points, connected by elastic elements in a triangular mesh (Fig. 1). The position $\mathbf{r}_{\mathrm{LP}}$ and the velocity $\mathbf{v}_{\mathrm{LP}}$ of each particle are governed by Newton's laws of motion:

$$\frac{\mathrm{d}\mathbf{v}_{\mathrm{LP}}}{\mathrm{d}t} = \frac{\sum_i \mathbf{F}_i}{m}, \quad \frac{\mathrm{d}\mathbf{r}_{\mathrm{LP}}}{\mathrm{d}t} = \mathbf{v}_{\mathrm{LP}}, \tag{5}$$

where $\sum_i \mathbf{F}_i = \mathbf{F}_{\mathrm{elast}} + \mathbf{F}_{\mathrm{int}} + \mathbf{F}_{\mathrm{visc}}$ is the total force exerted on the i-th particle. It consists of the elastic forces from neighboring particles in the membrane of the same cell (bonded interactions), the forces of non-bonded interactions with other cells, boundaries and polymers and viscous drag forces from the fluid.

The elastic model of each blood cell accounted for stretching elasticity, bending rigidity, conservation of volume and surface: $\mathbf{F}_{\mathrm{elast}} = \mathbf{F}_{\mathrm{sp}} + \mathbf{F}_{\mathrm{b}} + \mathbf{F}_{\mathrm{a}} + \mathbf{F}_{\mathrm{v}}$, where

$$\mathbf{F}_{\mathrm{sp}} = \kappa_s \frac{\lambda^{0.5} + \lambda^{-2.5}}{\lambda + \lambda^{-3}} \frac{\Delta l}{l_0} \mathbf{n}, \tag{6}$$

$$\mathbf{F}_{\mathrm{b}} = \kappa_b \frac{\Delta\theta}{\theta_0} \mathbf{n}_b, \tag{7}$$

$$\mathbf{F}_{\mathrm{a}} = -\kappa_{\mathrm{al}} \frac{\Delta S_i}{(S_i^0)^{0.5}} \mathbf{w} - \kappa_{\mathrm{ag}} \frac{\Delta S_g}{S_g^0} \mathbf{w}, \tag{8}$$

$$\mathbf{F}_{\mathrm{v}} = -\kappa_v \frac{\Delta V}{V_0} S_i \mathbf{n}_b. \tag{9}$$

Here $\Delta l = l - l_0$ is the spring elongation relative to its equilibrium length l_0, $\lambda = l/l_0$, κ_s is the stretching spring constant, and $\mathbf{n}$ is the unit vector pointing from one membrane point at another; $\mathbf{n}_b$ is the unit vector normal to the triangle (pointing at the exterior of the capsule), $\Delta\theta$ is the angle deviation from θ_0, κ_b is the bending elasticity constant; $\Delta S_i = S_i - S_i^0$ is the change of the i-th mesh triangle area, $\mathbf{w}$ is a unit vector pointing from the centroid of the triangle at the vertex, and ΔS_g is the global membrane area change; $\Delta V = V - V_0$ is the volume change. The force $\mathbf{F}_{\mathrm{b}}$ is applied to the vertex not belonging to the common edge of adjacent triangles, and the opposite force divided by two was applied to the two vertices lying on the common edge. The area conservation force $\mathbf{F}_{\mathrm{a}}$ is symmetrically applied to all vertices in plane of each triangle. The volume conservation force $\mathbf{F}_{\mathrm{v}}$ is calculated for each i-th triangle with area S_i and is evenly distributed over its vertices.

The platelets were assumed hardly deformable (though not absolutely solid), as it follows from real-life observations for inactive circulating platelets. The dimensionless elastic parameters for the present study were chosen as follows: $\kappa_s = 10.0$, $\kappa_b = 0.1$, $\kappa_{al} = 1.0$, $\kappa_{ag} = 1.0$ and $\kappa_v = 1.0$ in dimensionless units.

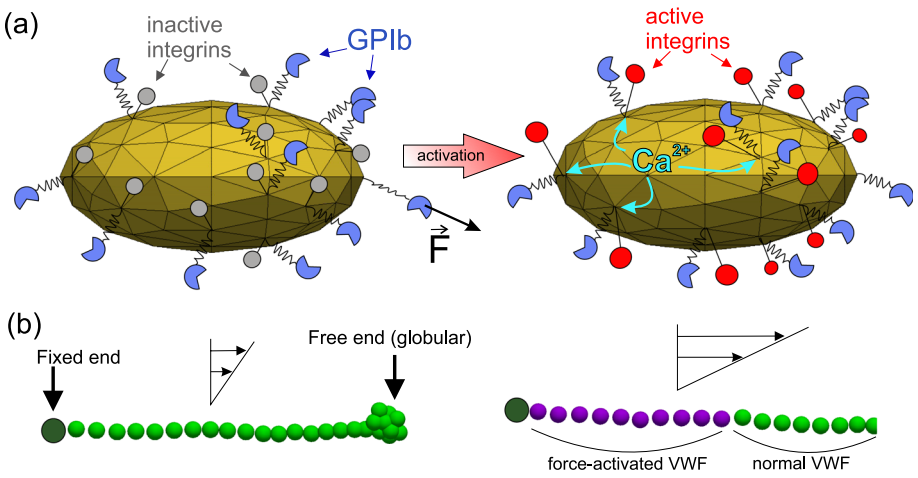

Fig. 1 Schematic representation of platelets, von Willebrand factor (VWF) and the concepts of mechanical activation events. **a** A platelet contains numerous GPIb receptors on its outer membrane (blue) that are always ready to bind its specific ligand - VWF. At the same time, $\alpha_{\mathrm{IIb}}\beta_3$ integrins are also present on the membranes of circulating platelets in the inactive state (gray), unable to bind neither fibrinogen, nor VWF. Several stimuli, mainly stretching force on GPIb receptors, may cause an increase in calcium level in cytosol, and subsequent transition of $\alpha_{\mathrm{IIb}}\beta_3$ into active conformation (red). **b** VWF multimers in low-shear conditions are normally present in the auto-inhibited, low-affinity state. Stretching force exceeding a known threshold causes conformational changes in VWF, providing its transition to active (magenta) state with an increased affinity to GPIb platelet receptors. (Color figure online)

The adhesive receptors GPIb were modeled as Lagrangian particles attached to the platelet membrane particles via harmonic springs:

$$U_{\mathrm{GPIb}}^{\mathrm{elastic}}(r) = \frac{1}{2}\kappa_{\mathrm{GPIb}} r^2. \tag{10}$$

Such approach was needed in order to measure the force exerted on platelet GPIb receptors during a simulation run. Here the stiffness of the linker peptide κ_{GPIb}. In fact, as we study here the force-induced MSD infolding, the only important value is the tension that stretches this linker, but not its actual length. Therefore, for the aims of the present paper this parameter was taken to be approximately equal to the stiffness of the VWF inter-monomer bond κ_{VWF}.

The integrin receptors $\alpha_{\mathrm{IIb}}\beta_3$ in our model were represented by virtual sites, linked to each platelet membrane particle by a distance-based condition. Thus, $\alpha_{\mathrm{IIb}}\beta_3$ beads can interact with other particles in the system, yet their positions are not obtained by integrating the equations of motion. This model assumption reflects the fact that integrin proteins are linked to the cytoskeleton of blood platelets via filamin, Ozaki et al. (2005).

2.4 Coupling between the particles and the fluid

The coupling between the particles and fluid was achieved via the well-established viscous coupling method with thermal fluctuations (Dünweg and Ladd (2009); Giupponi et al. (2007); Ahlrichs and Dünweg (1999)). A viscous drag force on a bead (representing either platelet membrane point, or a VWF monomer) was taken to be proportional to the local velocity difference between the bead and the fluid, $\mathbf{F}_{\mathrm{visc}} = -\xi(\mathbf{v}_{\mathrm{LP}} - \mathbf{v}_{\mathrm{fl}})$, and the opposite force was transferred back to the fluid. The parameter of friction ξ was adjusted from a special calibration procedure (Belyaev (2017)) individually for each kind of beads in the simulations: for the dynamic viscosity $\mu = 0.003\,Pa \cdot s$ for the platelet membrane particles $\xi_{\mathrm{plt}} = 0.43 \cdot 10^{-9}\,N \cdot s/m$ and for VWF monomers $\xi_{\mathrm{VWF}} = 0.5 \cdot 10^{-9}\,N \cdot s/m$ (both active and inactive). These values are supposed to change proportionally to μ in our model. Since GPIb receptors were represented by particles, for them we introduced the friction coefficient as well, $\xi_{\mathrm{GPIb}} = 0.25\xi_{\mathrm{plt}}$. For the integrins $\alpha_{\mathrm{IIb}}\beta_3$ the friction coefficient was set to zero because these receptors were modeled as virtual sites linked to the platelet membrane particles by a geometrical constraint, thus their effect on hydrodynamic properties of the platelets was negligible. The validation of cell-fluid coupling for platelets was based on the calculation of drag forces and torques experienced by a platelet in a shear flow near a plane wall (Belyaev (2018, 2017)), as well as for the VWF monomers in the shear flow (Kushchenko and Belyaev (2020)).

2.5 Non-bonded physical interactions

Unlike, the viscous friction forces described above, the non-bonded interactions between the Lagrangian particles were represented by potential forces derived from corresponding potential energies, $\mathbf{F}_{\mathrm{int}} = -\nabla \sum U(r)$. This sum consists of the following contributions.

The adhesive interactions between VWF monomers and platelet receptors GPIb, as well as $\alpha_{\mathrm{IIb}}\beta_3$, were modeled by Morse potential:

$$U_i^s(r) = A_i^s \cdot \left[\{1 - e^{-\alpha(r-r_{\mathrm{min}})}\}^2 - 1\right]. \tag{11}$$

Here the subscript i denotes the receptor type, and the superscript "s" denotes the distinction in the adhesion energy between the active and the inactive states of respective interacting particles, see Table 1; r is the distance between the centers of interacting beads; $\alpha = 100$, $r_{\mathrm{min}} = r_0 = 2a$. This potential was truncated at $r_{\mathrm{cut}} = 3a$. The values A^s_{GPIb} were considered as free parameters in this study, varied in range from $2kT$ to $200kT$, in order to investigate the effect of mutability of adhesive proteins on primary platelet adhesion to VWF.

The inter-monomer attractions between the VWF monomers, which are responsible for the compact conformation of the multimers at low shear, were introduced each VWF bead in a way similar to Schneider et al. (2007); Kushchenko and Belyaev (2020); Schwarzl and Netz (2018) by using Lennard-Jones potential (truncated at $r_{\mathrm{cut}} = 2r_0 = 4a$ and shifted to zero at the truncation point)

$$U_{\mathrm{VWF-VWF}}(r) = 4\epsilon\left[\left(\frac{\sigma}{r}\right)^{12} - \left(\frac{\sigma}{r}\right)^{6}\right] + U_{\mathrm{shift}} \tag{12}$$

with $\sigma = 2^{-1/6} r_0$ and $\epsilon = 4kT$, following our prior validation studies (Kushchenko and Belyaev (2020); Belyaev (2018, 2019)). This potential was used regardless of the activation state of VWF monomers.

Soft sphere short-range repulsion was introduced to avoid penetration of the walls and cells by particles. Between for each VWF bead the following potentials were assigned:

Table 1 Adhesive interactions between platelet receptors and VWF monomers

Type 1	Type 2	A_i^s	α	r_{min}	r_{cut}
GPIb	inact. VWF	A^{na}_{GPIb}	100	$2a$	$3a$
GPIb	act. VWF	$A^{\mathrm{act}}_{\mathrm{GPIb}}$	100	$2a$	$3a$
inact. $\alpha_{\mathrm{IIb}}\beta_3$	any VWF	0	–	–	–
act. $\alpha_{\mathrm{IIb}}\beta_3$	any VWF	A_{int}	100	$2a$	$3a$
act. $\alpha_{\mathrm{IIb}}\beta_3$	act. $\alpha_{\mathrm{IIb}}\beta_3$	$A^{\mathrm{self}}_{\mathrm{int}}$	100	$2a$	$3a$
GPIb	any $\alpha_{\mathrm{IIb}}\beta_3$	0	–	–	–
GPIb	GPIb	0	–	–	–

$$U^{\text{rep}}(r) = U_0^{\text{rep}} \cdot (r - r_{\text{off}})^{-n}, \tag{13}$$

where r is the distance between two beads or between a bead and a wall boundary, r_{off} is the off-set introduced to avoid singularities, n is the index, see Table 2.The cutoff r_{off} radius was also introduced for each repulsive interaction. Any change in the activation state of VWF monomers and $\alpha_{\text{IIb}}\beta_3$ receptors had no effects on the repulsion, according to the model assumptions.

Table 2 Repulsive non-bonded interactions, Eq. (13), between particles of different types and/or boundaries

Type 1	Type 2	U_0^{rep}	n	r_{cut}	r_{off}
VWF	Wall[1]	10^{-3}	1.2	$2a$	0
VWF	Plt[2]	0	1.2	$2a$	0
Plt	Wall	10^{-5}	2.0	0.3	−0.2
Plt	Plt[3]	10^{-3}	2.0	0.8	−0.5
GPIb	Wall	10^{-5}	1.2	$2a$	0
$\alpha_{\text{IIb}}\beta_3$	Wall	10^{-5}	1.2	$2a$	0

[1] Wall—top and bottom boundaries of the box.

[2] Plt—platelet membrane particles, not to be confused with the receptor particles.

[3] Here we exclude those platelet particles (pairs) that belong to the same platelet

2.6 Simulation protocol

A single time step scheme was chosen in the present implementation of the model $\Delta t = \Delta t_{LB} = \Delta t_p = 1/350$ [t], allowing for stable and accurate simulations of platelet and VWF dynamics in high wall shear stress conditions. According to our tests, any further decrease in the timestep did not result in any detectable changes.

Before each simulation run, the polymers multimers were attached to the bottom surface of the simulation box and equilibrated (Fig. 2). The blood cells (platelets) were placed near the wall at a certain distance in the beginning of each run. The density and size of VWF multimers were the same for each run: 100 polymer chains consisting of 30 monomers were randomly placed over the bottom wall area $16 \times 16\,\mu\text{m}^2$.

Initially the platelets were distributed so that their centers were located in the plane parallel to the bottom wall of the simulation box. The distance between each platelet membrane and the bottom wall was the same. Within that plane the centers of the platelets were distributed in random positions, bearing in mind that platelets should not overlap. The tethering points for the VWF multimers were also randomly

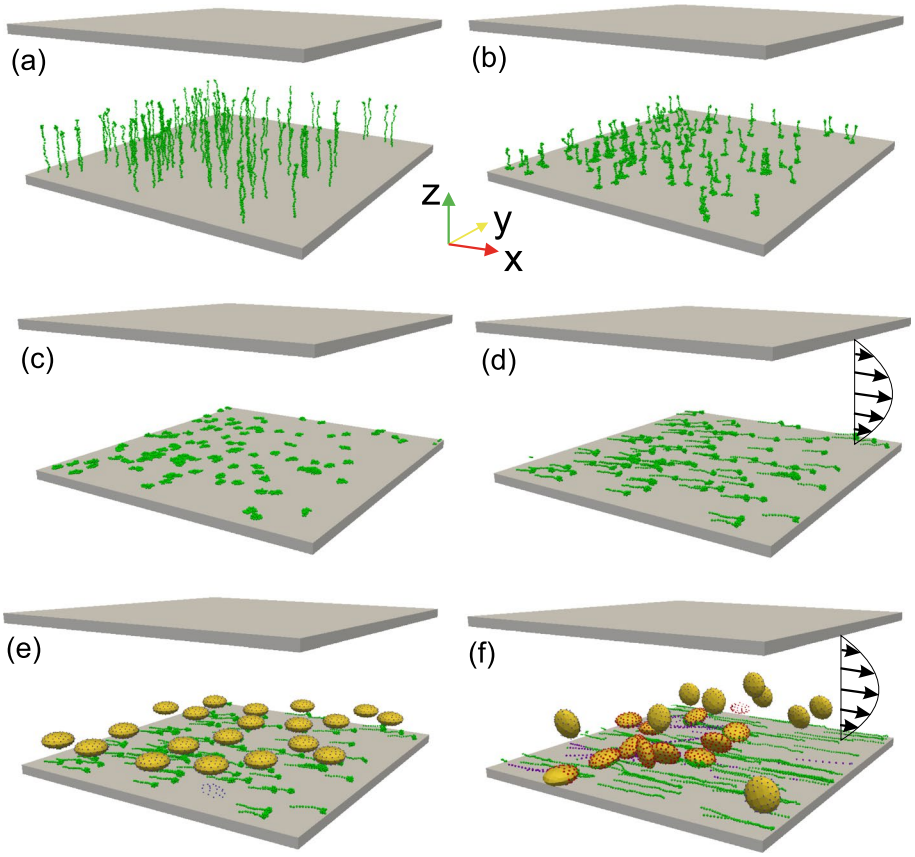

Fig. 2 Scheme of the simulation box and illustration of the simulation protocol. **a** The VWF multimers in the linear conformation were placed normally to the bottom wall of the system (randomly distributed) and position of the proximal monomer was fixed. **b** During the equilibration procedure in steady thermalized LB fluid the VWFs turn into the compact conformation **c** due to effective inter-monomer attraction. **d** After that the VWFs were subjected to the pressure-driven flow (without platelets) during 5 ms of physical time. **e** The platelets were placed into the system after the equilibration of VWFs. **f** After that the productive simulations with pressure-driven flow begun. Here the blue beads indicate GPIb receptors on platelets, and the red beads correspond to active $\alpha_{\text{IIb}}\beta_3$ receptors

distributed. To avoid any possible artifacts related to the initial placement, several independent simulation runs were performed for each reported set of parameters.

The calculations were performed on the supercomputer "Lomonosov-2" (Sadovnichy et al. (2013); Voevodin et al. (2019)) with 8 CPUs per each run, and it took ≈ 60 min to simulate 100 ms of physical time for a system with 20 platelets and 100 VWF chains in $16 \times 16 \times 8\,\mu m^3$ box.

3 Results

3.1 Validation of the model

The model the VWF multimers has been validated in our prior papers by comparing the simulation results for individual VWF chains (Belyaev (2018); Kushchenko and Belyaev (2020); Belyaev (2019)) with available experimental data by Fu et al. (2017). In these simulations we investigated the dynamics of both grafted and free-flowing VWF chains, studied their elongation and tension on each inter-monomer spring depending on length of the chains, drag coefficient and the strength of non-bonded inter-monomer interactions. The hydrodynamic properties were tuned from this comparison so that the modeled individual VWF chain accurately reproduces the experiments, in particular, the threshold of WSS for VWF uncoiling and activation (Kushchenko and Belyaev (2020)). The hydrodynamic properties of the modeled platelets were also accurately tuned in order to comply with known theoretical expressions for drag force and torque on the particles immersed in a sheared viscous Newtonian fluid near a plane wall (Belyaev (2018, 2018, 2017)). We also ensured that ellipsoidal platelets reproduce the expected and well-described dynamics in absence of adhesive interactions and boundaries, i.e., Jeffery's orbits. These validation data was published earlier in Belyaev (2017).

For the purpose of validation of new features implemented in the present work, mainly concerning platelet recruitment to wall-grafted VWF with shear-switchable adhesivity, here we present the comparison between our simulations and corresponding experimental data by Schaff et al. (2013); Kulkarni et al. (2000); Shi et al. (2016). Among found published results, here we use only the data obtained via the flow-chamber technique with surface-immobilized wild-type VWF multimers, as the simulations were meant to reproduce this particular setup. Figure 3 demonstrates the validity of the proposed approach, as the model reproduces experimental observations. In particular, we meet quantitative agreement with the data reported in Schaff et al. (2013) (Fig. 3a). However, the number of adherent platelets may depend on the density of wall-grafted VWF multimers, thrombocrit, exposure time, experimental protocol, etc. Therefore, in the cases of Kulkarni et al. (2000); Shi et al. (2016), with which the simulations demonstrate qualitative agreement, the adherent platelet density was normalized with respect to the maximum value (Fig. 3b). The data by Shi et al. (2016) is better described if we imply the activatable $\alpha_{IIb}\beta_3$ integrins in the simulations. The experimental data is better predicted by the simulation results if $F_{actVWF} = 10 - 20$ pN and $A^{na}_{GPIb} = 2kT$, $A^{act}_{GPIb} = 200kT$ —these parameters were used as reference values for the wild-type VWF in the present work.

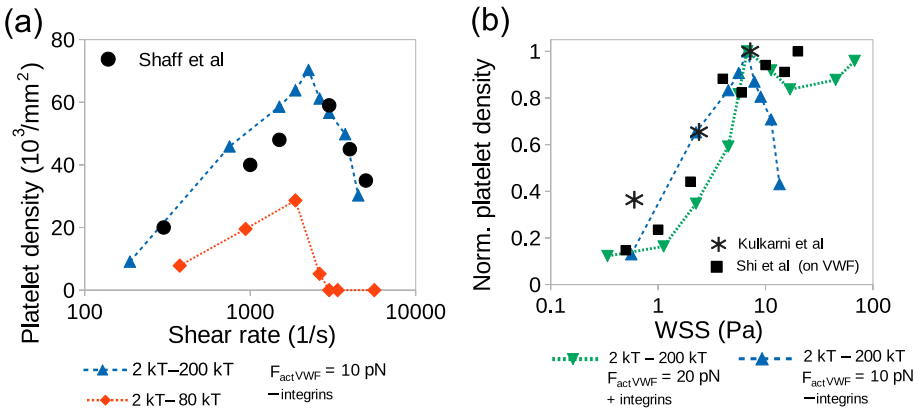

Fig. 3 The comparison of several simulations with experimental data found in literature Schaff et al. (2013); Kulkarni et al. (2000); Shi et al. (2016). **a** Surface density of adherent platelets vs. the wall shear rate: circles—experiments from Schaff et al. (2013), triangles and diamonds with dashes lines—simulations of the present work with inactive/inhibited $\alpha_{IIb}\beta_3$ integrins ($A_{int} = A^{self}_{int} = 0$). The activatable VWF model was used with $A^{na}_{GPIb} = 2kT$, $A^{act}_{GPIb} = 200kT$ (triangles) and $A^{na}_{GPIb} = 2kT$, $A^{act}_{GPIb} = 80kT$ (diamonds). The VWF activation force was set to $F_{actVWF} = 10$ pN. **b** The qualitative comparison of normalized density of adherent platelets versus wall shear stress. The symbols—asterisks and squares—correspond to the experimental data from Kulkarni et al. (2000) and Shi et al. (2016), respectively. The triangles with dashed lines correspond to simulations with different parameter sets: $A^{na}_{GPIb} = 2kT$, $A^{act}_{GPIb} = 200kT$, $A_{int} = A^{self}_{int} = 0$, $F_{actVWF} = 10$ pN (the up-pointing ones), $A^{na}_{GPIb} = 2kT$, $A^{act}_{GPIb} = 200kT$, $A_{int} = 2A^{act}_{GPIb}$, $A^{self}_{int} = 0$, $F_{actVWF} = 20$ pN (the down-pointing ones). The lines on both panels are depicted only as visual cues

3.2 Tension force exerted on platelet GPIb receptors

In order to quantify the force exerted on platelet GPIb receptors during initial adhesion in various hydrodynamic conditions, we performed a set of additional simulation runs with only one platelet (to avoid interference from platelet-platelet collisions and collective effects) and 50 grafted VWF multimers in a smaller simulation box ($16 \times 8 \times 8\ \mu m^3$). For various WSS and different values of adhesion parameters we measured the maximal tension force among all the receptors present on the surface of the modeled platelet, then averaged this value over the simulation time for each particular run (Fig. 4a–c). Additionally, the average velocity of the platelet's center of mass was also calculated during the post-processing, as a criterion for the stable platelet adhesion (Fig. 4d–f). In case of activatable VWF (considered in these simulations) the extreme forces on GPIb receptors exceed $10 - 20\ pN$—the critical value for MSD unfolding reported in Deng et al. (2016); Zhang et al. (2019)—if the wall shear stress $\geq 4\ Pa$. The platelets adhere to VWF in a range of WSS, depending on the binding energy between GPIB and the non-activated VWF monomers, as described above. For the non-activatable VWF with a moderate binding energy ($A_{\mathrm{GPIb}} = 40kT$) the critical tension is hardly reached for WSS $= 4\ Pa$ and remains below $10\ pN$, while the platelet tethering was only observed under low shear.

These simulation results show that the drag force exerted on a platelet tethered to a wall may significantly exceed the characteristic MSD unfolding force under physiological or elevated shear stress. Therefore, the mechanical stimulation of platelet GPIb receptors is highly plausible to cause the outside-in signaling and further activate $\alpha_{\mathrm{IIb}}\beta_3$ via mechanotransduction pathway. It does not require chemical agonists (neither ADP, nor thromboxane A2, nor thrombin) to be present in the vicinity of the channel wall—only reliably attached VWF multimers and relevant hydrodynamic conditions are needed for platelet activation. This finding derived from our theoretical study is important for the analysis of platelet aggregation in microfluidic flow chambers (in vitro), as well as for understanding of the initial stages of microvascular thrombosis in vivo.

By altering the number of grafted VWFs in the simulations, we have studied the changes in the tension of the GPIb receptors with respect to the number of bonds between a

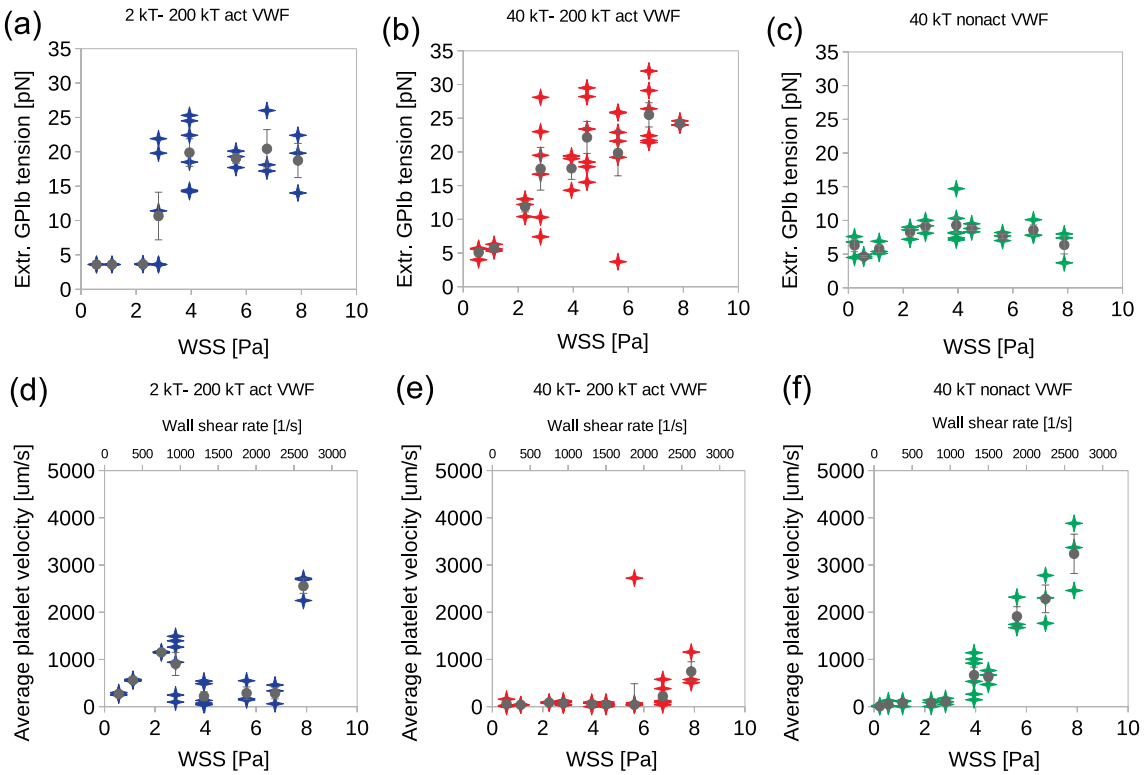

Fig. 4 **a-c** Extreme value of the tension force exerted on platelet GPIb receptors in the model as a function of the hydrodynamic wall shear stress. The extreme force was measured as the maximal tension force among all GPIb receptors of the platelet, then this value was averaged over the simulation time. In these simulations 1 platelet and 50 VWF multimers (30-mers) were used. For each wall shear stress, up to 6 independent runs were performed, each run is depicted as a "star" symbol. The mean values are denoted as gray dots, while the errors bars depict the standard error. **d-f** The average velocity of a platelet measured in these simulations. The following parameters were used: dynamic viscosity of the fluid $\eta = 0.003$ Pa·s; VWF activation force $F_{\mathrm{actVWF}} = 35$ pN

platelet and the tethered VWF multimers (see the Supplementary Text file, Figures S1, S2 and S3 and the comments therein). When we increased twofold the density of VWFs, the number of bonds between the platelet and the wall was greater, and it led to a slight decrease in the maximum force magnitude (over the ensemble of GPIb receptors belonging to the same platelet) from 25 to 21 pN, which was not significant for the main conclusions of the paper. When we decreased the number of tethered VWFs twofold under the same hydrodynamic conditions and for the same parameters, the platelet was unable to adhere stably, but formed transient bonds with the surface, and the peak value was noticeably higher than in the reference case. We inspected the distribution of the tension force among the GPIb receptors in simulations. It was found that the tension is distributed heterogeneously among the GPIb receptors that actually formed bonds with VWF. Even in the steady case, some bonds are forced above the activation threshold, while others experience much smaller forces.

There are two additional factors consider. Firstly, the steady-state force value is lower than the instantaneous value of the jerk force exerted on GPIb receptors at the beginning of platelet's deceleration stage. Thus, the MSD unfolding and the consequential integrin activation may in principle be triggered before the platelet stops. Secondly, collisions of adherent platelets with free cells can cause instantaneous peaks in the bond tension, which again may exceed the activation threshold. This may become more pronounced in narrow vessels with RBCs present in the flow, yet it requires a particular study in future.

3.3 Effect of VWF activation on platelet adhesion

We compared the capability of activatable and non-activatable VWF multimers to catch and hold platelets near the wall in a viscous fluid flow. For this a series of simulations for different values of the parameters $A^{\mathrm{act}}_{\mathrm{GPIb}}$ and A^{na}_{GPIb} were performed in different hydrodynamic conditions, characterized by the wall shear stress (WSS) and, equivalently, the Reynolds number Re. In this part, the integrins $\alpha_{\mathrm{IIb}}\beta_3$ were assumed inhibited (inactive) in the simulations, and only the GPIb contributed to platelet adhesion. For each set of parameters we performed at least 3 independent simulation runs with random initial localization of VWF multimers on the bottom wall. For each run 100 VWF multimers were grafted to the wall. The platelet were also randomly placed so that the distance between the wall and each platelet's center of mass was kept the same (equal to 1 μm). During each run at least 100 ms were simulated to ensure that the number of adherent platelets doesn't significantly change in time after reaching the steady state. We note that for the slower flows ($Re < 10^{-3}$, corresponding to WSS < 0.5 Pa) it required 200 ms to reach the equilibrium, while for the faster flow ($Re > 10^{-2}$, WSS > 5 Pa) it took less that 50 ms. In all these simulations the dynamic viscosity of the fluid was set to 0.003 $Pa \cdot s$ and kept the same with the appropriate choice of the friction coefficients for the platelets and the VWF multimers. The hydrodynamic conditions corresponded to the plane Poiseuille flow with $10^{-4} < Re < 3 \cdot 10^{-2}$, which is equivalent to wall shear stress 0.05625 $Pa < WSS < 16.875$ Pa in the simulation box described in the Methods section.

The simulation results in Fig. 5a illustrate the effect of variation of the adhesive potential amplitude on the number of adherent platelets for the non-activatable VWF (i.e., $A^{\mathrm{act}}_{\mathrm{GPIb}} = A^{na}_{\mathrm{GPIb}} = A_{\mathrm{GPIb}}$). The behavior of the model is quite expected in this case: the greater the value of A_{GPIb}, the greater shear rate adherent platelets can withstand. At the same time, for the lower values of the WSS, the number of adherent platelets is almost independent from the hydrodynamic conditions and thus can be only regulated by the rate of platelet collisions with VWF multimers.

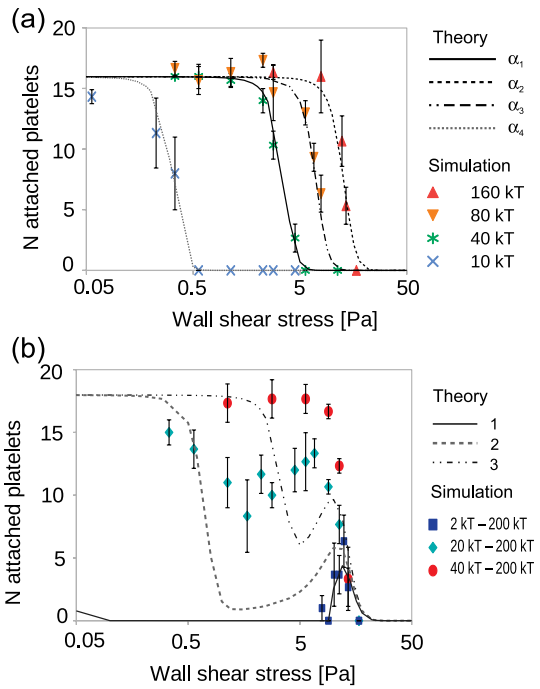

Fig. 5 Number of platelets that remain adherent to VWF after first 100 ms of the simulations versus the wall shear stress for **a** non-activatable ($A^{na}_{\mathrm{GPIb}} = A^{\mathrm{act}}_{\mathrm{GPIb}} = A_{\mathrm{GPIb}}$) and **b** activatable VWF multimers ($A^{na}_{\mathrm{GPIb}} \neq A^{\mathrm{act}}_{\mathrm{GPIb}}$). **a** The symbols correspond to the respective values of A_{GPIb} used in the model, see legend. The lines correspond to theoretical estimation with Eq. (14) with $\alpha_1 = 2$, $\alpha_2 = 0.55$, $\alpha_3 = 1$, and $\alpha_4 = 22$. **b** The symbols correspond to the simulations, each legend entry reads as "$A^{na}_{\mathrm{GPIb}} - A^{\mathrm{act}}_{\mathrm{GPIb}}$." The lines correspond to Eq. (20): $\alpha_{\mathrm{act}} = 0.55$, $K = 0.001$, $N_0 = 18$; $\alpha_{\mathrm{na}} = 200$, 10 and 2 for lines "1," "2" and "3", respectively. Here $F_{\mathrm{actVWF}} = 35$ pN for both panels. In all panels the symbols indicate the average value for 3 independent simulation runs, the error bars is the standard error

The simulated data were fitted with theoretical curves, see Appendix 1:

$$N_{\mathrm{adh}}^{\mathrm{theor}} = \frac{N_0}{1 + K \cdot \exp(\alpha \cdot WSS)}, \tag{14}$$

where for this set of simulations $N_0 = 16$, $K = 0.001$, and α depends on the binding energy A_{GPIb}. In Fig. 5a, α is the fitting parameter. We see that the simulations agree with the theory in this case, suggesting that depth of the adhesive potential well A_{GPIb} is the main parameter that controls platelet binding in this regime of the model.

In contrast, for the activatable VWF (i.e., $A_{\mathrm{GPIb}}^{\mathrm{act}} \neq A_{\mathrm{GPIb}}^{na}$) the number of activated VWF monomers grows with the wall shear stress, as well as the number of the adhering platelets (Fig. 5b). Here, the parameter α_{na} (see Appendix 1, Eq. 20) is the fitting parameter. This effect of shear-induced activation of VWF is much more pronounced when the energy of a deactivated VWF monomer A_{GPIb}^{na} is almost negligible ($A_{\mathrm{GPIb}}^{na} = 2\,kT$), while the adhesion to an activated VWF monomer is rather strong ($A_{\mathrm{GPIb}}^{\mathrm{act}} = 200\,kT$). The intermediate case ($A_{\mathrm{GPIb}}^{na} = 20\,kT$, $A_{\mathrm{GPIb}}^{\mathrm{act}} = 200\,kT$) demonstrates a non-monotonous dependence between the platelet adhesivity and WSS, clearly explained by the enforcement of the adhesion forces due to the increasing number of high-affinity bonds (GPIb-active VWF) as the WSS increases. In other words, weak bonds (GPIb-deactivated VWF) work at low WSS, while the high-affinity bonds take over upon the VWF activation. The abnormally strong bonds between GPIb and deactivated VWF monomers may neglect the protecting self-inhibitory effect of VWF monomers at low WSS (for instance, $A_{\mathrm{GPIb}}^{na} = 40\,kT$, $A_{\mathrm{GPIb}}^{\mathrm{act}} = 200\,kT$), presumably leading to undesired platelet aggregation in normal hemodynamic conditions. Such a behavior of the model is similar to the effects that takes place in case of mutations causing von Willebrand disease type 2B (Ruggeri et al. (1980)) or under the action of botrocetin (Deng et al. (2016); Fukuda et al. (2005)).

For the case of the activatable VWF multimers, we used different values of the critical tension force F_{actVWF} required for the activation of a VWF monomer (10, 20 and 35 pN) in order to study the effect of this parameter on platelet adhesion—the results are presented in Fig. 6a. The number of attached platelets correlates with the number of active VWF monomers present on the channel wall. The latter depends on the WSS in a threshold manner (Fig. 6b). The decrease in F_{actVWF} shifts down the threshold WSS for VWF activation as well as the onset of platelet adhesion, while the upper WSS threshold is controlled by the binding energy $A_{\mathrm{GPIb}}^{\mathrm{act}}$ between platelet receptors GPIb and activated VWF monomers. Thus, the parameter F_{actVWF} is the most important regulator of platelet adhesion (in case of activatable VWF. In Fig. 6c, we present the number

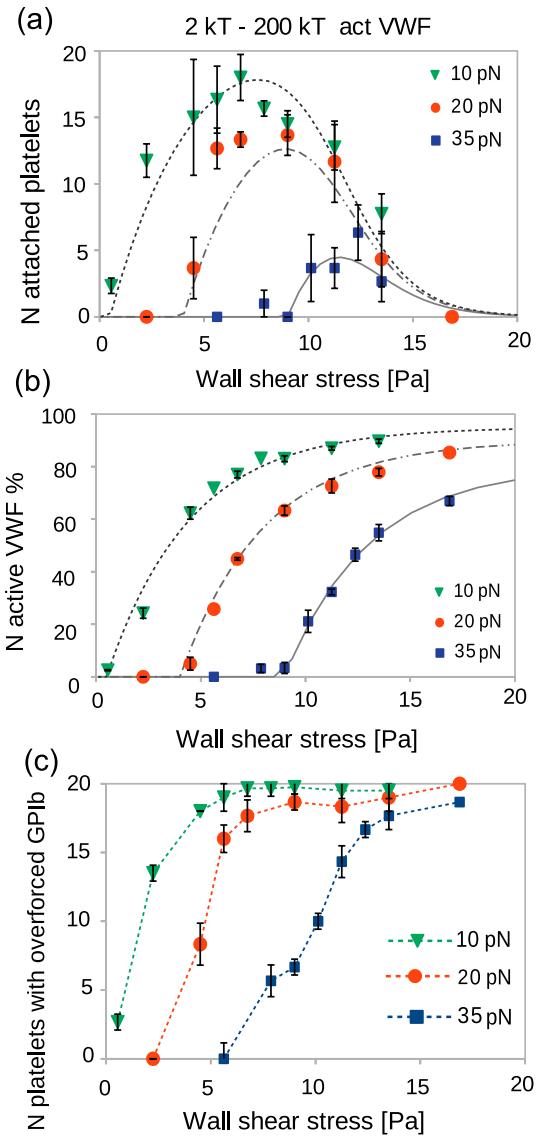

Fig. 6 The effect of the critical force F_{actVWF} required to activate the VWF subunits on platelet adhesion. The symbols correspond to simulations with $F_{\mathrm{actVWF}} = 10$ (triangles), 20 (circles) and 35 pN (squares) in all panels. Here $A_{\mathrm{GPIb}}^{na} = 2kT$, $A_{\mathrm{GPIb}}^{\mathrm{act}} = 200kT$, and the activation of integrins $\alpha_{\mathrm{IIb}}\beta_3$ was disabled. **a** The number of adherent platelets after 100 ms of simulations versus wall shear stress. The lines represent the theoretical estimations by Eqs.(21),(22) with $\mathrm{WSS}_* = 9$ Pa, $\varphi_0 = 0.8$ (solid); $\mathrm{WSS}_* = 4$ Pa, $\varphi_0 = 0.9$ (dash-dot) and $\mathrm{WSS}_* = 0.5$ Pa, $\varphi_0 = 0.95$ (dashed); $K = 0.001$, $\alpha_{\mathrm{act}} = 0.6$, $N_0 = 24$. **b** The percent of activated VWF monomers vs. wall shear stress; the lines correspond to Eq. (22) with the same parameters as in panel (**a**). **c** The number of platelets with overforced (≥ 10 pN) GPIb receptors versus wall shear stress; here the lines are only for the visual guidance. In all panels the symbols indicate the average over 3 independent simulation runs, the error bars is the standard error

of platelets, which GPIb receptors experience the tension force exceeding 10 pN - a characteristic force for uncoiling of its mechanosensitive domain (MSD). It can be seen that GPIb-mediated mechanical platelet activation correlates

with the shear-induced activation of VWF monomers and it may take place under moderate and, especially, high shear stress in the surrounding fluid (Fig. 7)

We also investigated the effect of the attractive energy A^{act}_{GPIb} (Fig. 8). The simulation results indicate that low affinity between platelet GPIb receptors and VWF multimers leads to low and even absent platelet adhesion, regardless of the number of activated VWF monomers and the number of overforced GPIb receptors. The model suggests that if the adhesive forces are not strong enough, then the initial hemostasis is hindered, but the mechanically activated platelets may be present in the bloodstream due to transient interactions between the platelets and the surface-grafted VWF.

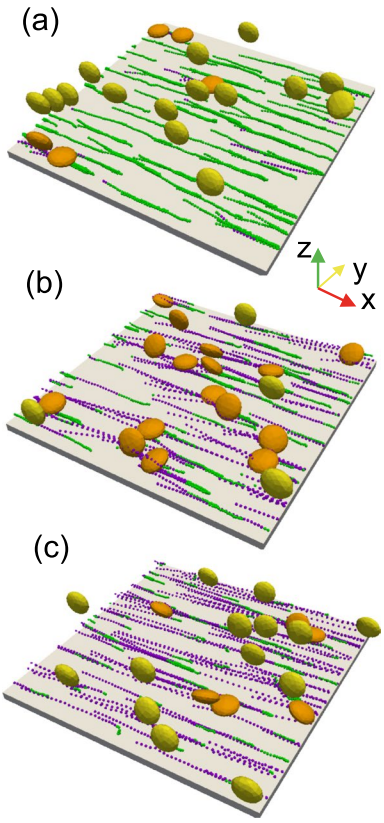

Fig. 7 The illustrative snap-shots from the simulations: **a** WSS = 4.5 Pa; **b** WSS = 9.0 Pa; **c** WSS = 13.5 Pa; $F_{actVWF} = 20$ pN, $A^{na}_{GPIb} = 2kT$, $A^{act}_{GPIb} = 200kT$, and the activation of integrins $\alpha_{IIb}\beta_3$ was disabled in the model. The steadily adherent platelets (with zero velocity of the center of mass) are depicted by the darker color, while the free-flowing ones—by the lighter color. The non-active and active VWF monomers are denoted by green and magenta beads, respectively. The top wall and platelet receptors are not shown for clear presentation

3.4 High affinity between platelet receptors GPIb and VWF monomers promotes both activation of VWF and MSD unfolding

Abnormally increased platelet aggregation rate under low shear stress, caused either by mutations or botrocetin, leads to platelet activation with consequent clearance, as observed in many experiments, e.g. Fukuda et al. (2005), Yago et al. (2008). The present simulations agree with these observations and show that abnormal affinity of GPIb to (inactive) VWF monomers may lead to early platelet activation, as illustrated by Fig. 9. The figure shows the number of platelets in the simulations, for which GPIb receptors experience the tension force $\geq 10\ pN$ and the unfolding of MSD may occur. The threshold WSS for MSD triggering is shifted down to 0.5-1 *Pa* in the case of strong binding between platelet receptors and VWF monomers for both activatable and non-activatable VWF models.

In contrast to that, if the attraction between (inactive) VWF and GPIb is low, the mechanosensitive domain is unlikely to unfold at WSS below 5 Pa, e.g., $A^{act}_{GPIb} = A^{na}_{GPIb} = 10kT$ in Fig. 9a or $A^{na}_{GPIb} = 2kT$, $A^{act}_{GPIb} = 200kT$ in Fig. 9b. Such behavior of the model complies with experimental observation that platelet rate of VWF-dependent adhesion drastically increases at WSS $\geq 5\ Pa$ and is negligible otherwise (Schneider et al. (2007)). The simulation results also qualitatively agree with experimentally measured fraction of shear-activated platelets from Shankaran et al. (2003); Dayananda et al. (2010). For the shear-induced platelet activation, caused by GPIb-mediated mechanotransduction, two factors should be met at the same time: the wall shear stress should be high enough to provide VWF uncoiling and VWF monomer activation, and binding between GPIb and VWF should be strong enough to withstand the hydrodynamic drag. The cascade of activation phenomena, probably, serves as a multi-stage protection against unnecessary aggregation of platelets in the bloodflow and, at the same time, for the amplification of platelet adhesion by involvement of $\alpha_{IIb}\beta_3$ at sites of inflammation or vascular damage.

In case of high binding energy A^{na}_{GPIb} between GPIb and inactive VWF monomers, further activation of VWF is augmented by platelet tethering to the wall-grafted VWF multimers (Fig. 10). The tensile forces on VWF in this case are comprised of a viscous drag on the monomers and a hydrodynamic force on the tethered platelet, thus the mechanical load on the upstream VWF monomers increases greatly upon adhesion of a platelet. This is illustrated by Fig. 11, where three simulation sets for $A^{na}_{GPIb} = 2$, 20 and $40kT$ are compared. Upon increase in the binding energy between GPIb and inactive VWF we encountered a significant amount of active VWF monomers at much lower WSS values in the simulations.

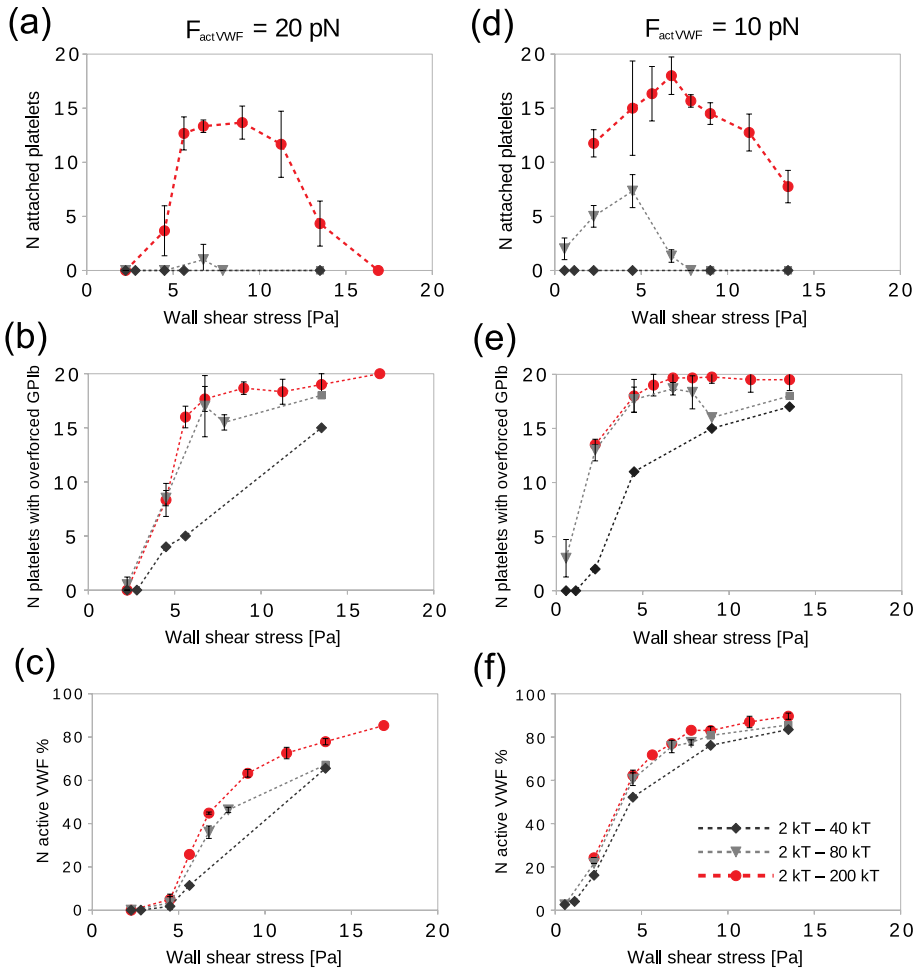

Fig. 8 Effect of F_{actVWF} and $A^{\mathrm{act}}_{\mathrm{GPIb}}$ on platelet adhesion dynamics in the simulations. Here $F_{\mathrm{actVWF}} = 10$ pN (**a-c**), and 20 pN (**d-f**). The number of adherent platelets (a,d), the number of platelets with overforced (≥ 10 pN) GPIb receptors and the percent of activated VWF monomers are plotted versus the wall shear stress. Symbols correspond to the simulated values averaged over 3 independent runs and the connecting lines serve only for visual guidance. The error bars is the standard error. Here $A^{\mathrm{act}}_{\mathrm{GPIb}} = 40kT$ (diamonds), $80kT$ (triangles) and $200kT$ (circles); $A^{na}_{\mathrm{GPIb}} = 2kT$, and the activation of integrins $\alpha_{\mathrm{IIb}}\beta_3$ was disabled

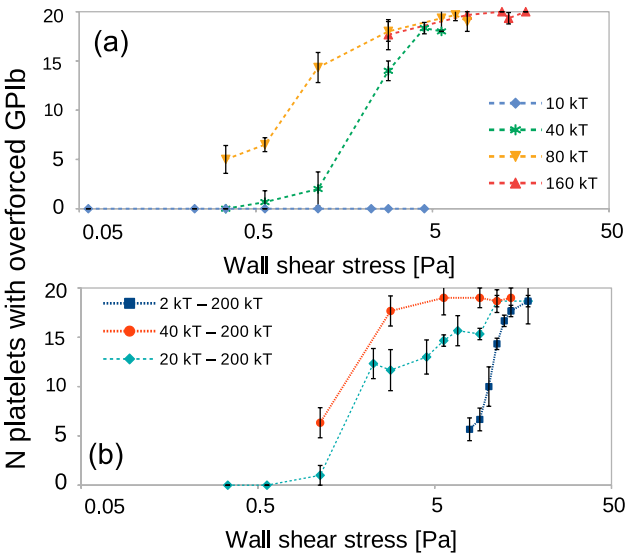

Fig. 9 Comparison of the number of platelets with overforced (≥ 10 pN) GPIb receptors in the simulations for **a** the non-activatable VWF ($A^{na}_{\mathrm{GPIb}} = A^{\mathrm{act}}_{\mathrm{GPIb}}$), and **b** the activatable VWF ($A^{na}_{\mathrm{GPIb}} \neq A^{\mathrm{act}}_{\mathrm{GPIb}}$). The legend is analogous to Fig. 5. The symbols indicate the average over 3 independent simulation runs, the error bars is the standard error, and the lines serve for visual guidance

The analysis of simulation results in Fig. 5b also suggests that VWF activation brings out some non-additive effects. Specifically, in terms of the attached platelets count, analytical fitting functions under-predict the simulation results. A probable explanation comes from the visualization of platelet positions at the end of the simulations (Fig. 12). We see that platelets accumulate in small groups, where the formerly attached ones provide additional number of active VWF monomers to bind in the upstream region, and also mechanically support those platelets that attach later in their upstream vicinity. Such groups of initially adherent platelets, subjected to consequent activation, ADP- or thromboxane A2-mediated inter-platelet signaling and spreading, may further form a nucleus of a platelet-rich thrombus.

3.5 Effect of $\alpha_{\mathrm{IIb}}\beta_3$ activation on platelet adhesion to wall-grafted VWF multimers

We further inspect the possibility of mechanical activation of platelet $\alpha_{\mathrm{IIb}}\beta_3$ receptors in various hydrodynamic conditions by implementing this mechanism into the model. Two phenomenological approaches were used. The first one is

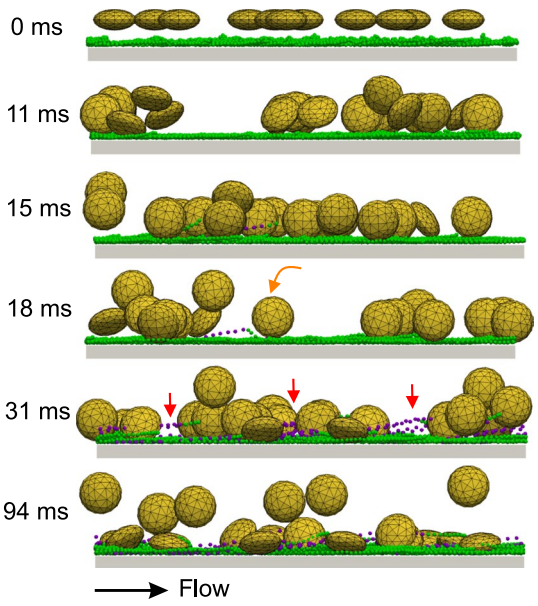

Fig. 10 Visualization of a simulation run in consequent moments of time after placing platelets into the box, a side view. The curved orange arrow indicates a platelet binding to a tethered VWF multimer, stretching it and lifting from the bottom wall due to adhesion forces between VWF monomers (magenta and green beads) and GPIb receptors (not shown). Smaller red arrows indicate numerous VWF multimers stretched and activated by the bound platelets

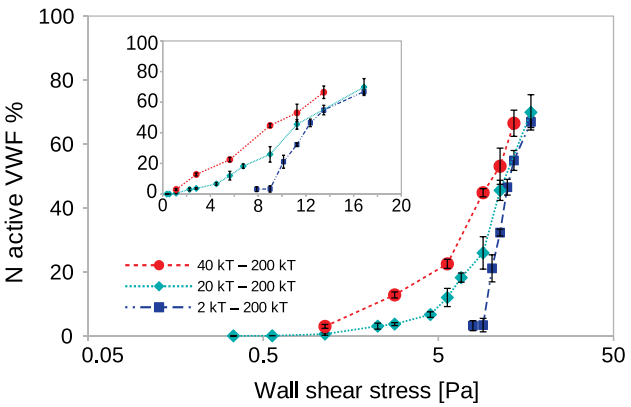

Fig. 11 Percent of activated VWF monomers in the simulation box after 100 ms of physical time as function of the wall shear stress for different affinity between the GPIb receptors and the inactive VWF monomers with log scale over the x-axis: $A^{na}_{\mathrm{GPIb}} = 2kT$ (blue line with squares), $20kT$ (green line with diamonds), $40kT$ (red line with circles). The lines serve for visual guidance, the symbols indicate the average over at least 3 independent simulation runs, the error bars indicate the standard error. The inset shows the same plot in linear scale

conditional: if the tension force exerted on a GPIb receptor of a platelet exceeds 10 *pN*, then this platelet is considered activated and all its membrane particles that represent $\alpha_{\mathrm{IIb}}\beta_3$ receptors turn into adhesive mode. The second, *stochastic* variant is based on experimental measurement of MSD unfolding rate, Zhang et al. (2015, 2019), depending on magnitude of the applied force F via Bell's law:

$$k_u = k_u^0 \cdot \exp\left(\frac{\sigma_{\mathrm{MSD}} F}{kT}\right), \tag{15}$$

where the unloaded unfolding rate $k_u^0 = 0.008\ s^{-1}$ and the barrier width $\sigma_{\mathrm{MSD}} = 2.6$ nm were taken from Zhang et al. (2015).

To reveal the consequences of the involvement of the $\alpha_{\mathrm{IIb}}\beta_3$ integrins in the process of initial platelet tethering to the wall with grafted VWF multimers, we performed simulations by means of thus modified model. Figure 13 summarizes the results for both implementations of the MSD unfolding kinetics. Regardless of the modeling details, we see that $\alpha_{\mathrm{IIb}}\beta_3$ supports platelet adhesion and activation under very high wall shear stress and does not affect platelet accumulation at low and moderate shear stress, where it is mainly governed by VWF activation due to hydrodynamic forces. The number of platelets that has been activated, but failed to adhere and so kept flowing with the blood by the end of each simulation, also increases as the WSS exceeds 5 *Pa*, but reaches its limit when the $\alpha_{\mathrm{IIb}}\beta_3$ receptors get involved.

Mechanical activation of platelets due to adhesion to VWF in shear flow indeed requires a reliable binding between GPIb receptors and A1 domain in VWF monomers. The change in adhesivity between them may affect this mechanism, so we altered the parameter $A^{\mathrm{act}}_{\mathrm{GPIb}}$ in the model to reveal its effect on platelet activation in our simulations (Fig. 14). The results indicate that the GPIB-VWF binding strength is indeed a crucial parameter, as diminished adhesivity of GPIb manifests in a lower number of activated platelets. If the binding energy $A^{\mathrm{act}}_{\mathrm{GPIb}}$ is high enough to cause MSD unfolding and initiate $\alpha_{\mathrm{IIb}}\beta_3$ activation, but not as strong as required to hold the platelets until $\alpha_{\mathrm{IIb}}\beta_3$ receptors form bonds with VWF, then the activated platelets detach from the substrate and travel with the blood flow. We also performed simulations for the case of the "non-activatable" VWF (as a model for VWD type 2B). As expected, such platelets in simulations had a tendency to get activated and to aggregate under lower WSS as compared to the normal ones. This agrees with current representation of the biophysical mechanism of this disorder: increased affinity of the Willebrand factor for platelets leads to rapid clearance of both the platelets and VWF from the plasma.

Therefore, GPIb-mediated platelet adhesion and consequent MSD-regulated mechanical activation should complement each other in order to function effectively and to avoid thrombotic conditions and embolization of activated platelets. The requirement of the effectiveness of initial platelet hemostatic reaction under optimal hydrodynamic conditions (WSS) demands the cooperativity between adhesion and

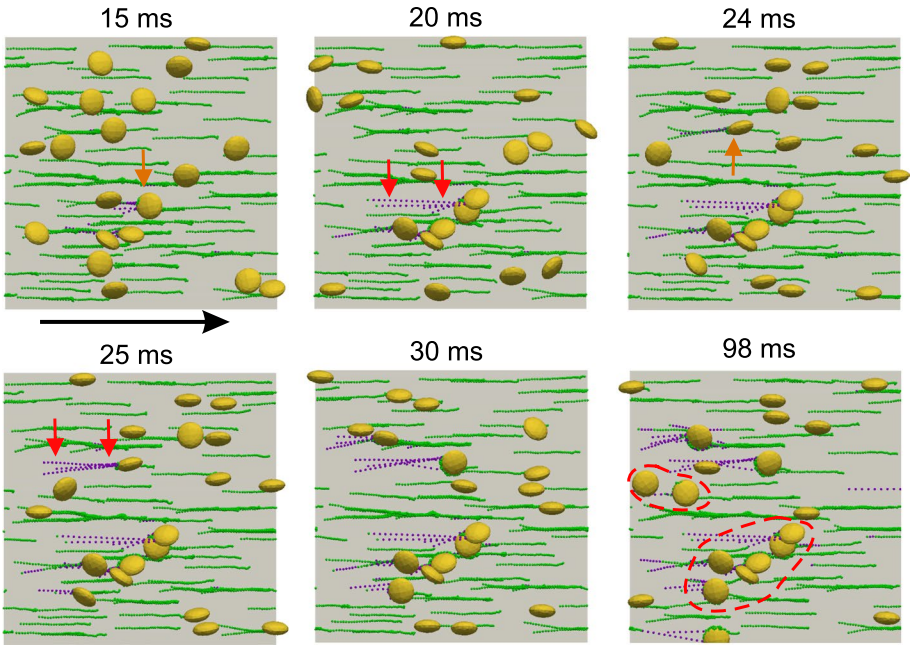

Fig. 12 Visualization of a typical simulation run at different moments of time, top view. The orange and red indicate platelets binding to VWF and thus the VWF monomers get activated by the stretching forces, mainly drag on these bound platelets. The black arrow indicated the flow direction. Initially, at time 15 ms, the VWF monomers are mostly inactive (green) and only a small number of active VWFs (magenta) is available for platelets. A random platelet binds to this portion of active VWFs (orange arrow) and in further moments (20 ms) stretches the whole bundle of four VWF multimers (red arrows). The same happens with another platelet (at 24 and 25 ms). The dashed closed lines at 98 ms indicate groups of platelets bound to the wall due to such additional, platelet adhesion-induced VWF activation

mechanotransduction in platelets. This idea is in agreement with recent findings of cooperative unfolding of two GPIb domains under mechanical tension: LRRD (leucine-rich repeat domain), which is responsible for adhesive bond lifetime prolongation, and the MSD that transduces a mechanical signal from the outer side of the membrane into a chemical stimulus inside the platelet (Ju et al. (2016)). The present theoretical study also demonstrates that by altering three key parameters of the system (the VWF activation force, the GPIb-VWF adhesion energy and the MSD infolding force), it may become possible to control the hemodynamic conditions, under which the platelet aggregation is most pronounced.

4 Discussion

The GPIb-mediated platelet adhesion to wall-grafted VWF multimers normally takes place in a certain range of hemodynamic conditions (expressed via WSS or shear rate). The computer simulations presented here suggest that the width of this range is controlled by two mechanical processes: the lower bound (the onset) of platelet adhesion is due to VWF stretching by hydrodynamic forces, while the upper bound is limited by the strength of adhesive interaction between GPIb receptors and activated VWF monomers. The fundamental nature and peculiarities of these biomechanical phenomena could be further unraveled by atomistic molecular dynamics of the involved proteins (e.g., the binding domain of GPIbα and the A1 domain of VWF) under mechanical load or hydrodynamic shear. Nowadays the atomistic MD simulations are possible for small parts of VWF, e.g., for the individual VWF domains or the complexes of VWF domains with platelets receptors. However, we believe that coarse-grained models, implicit solvent, metadynamics and the umbrella sampling technique can elucidate the mechanochemical features of VWF.

The presented simulations identify a cascade of mechanochemical activation phenomena that strengthen platelet aggregation and provide initial thrombogenesis as the wall shear stress increases: (1) VWF uncoiling under hydrodynamic forces, (2) VWF subunit activation, and (3) GPIb-mediated mechanotransduction. This sequence leads to activation of platelet integrins $\alpha_{\mathrm{IIb}}\beta_3$ that support the thrombus growth under high WSS conditions. Interestingly, the present simulation results suggest that $\alpha_{\mathrm{IIb}}\beta_3$ receptors may get activated via mechanical pathway even at moderate WSS. These conclusions are consistent with prior experimental observations of Ca^{2+} concentration in cytosol of platelets

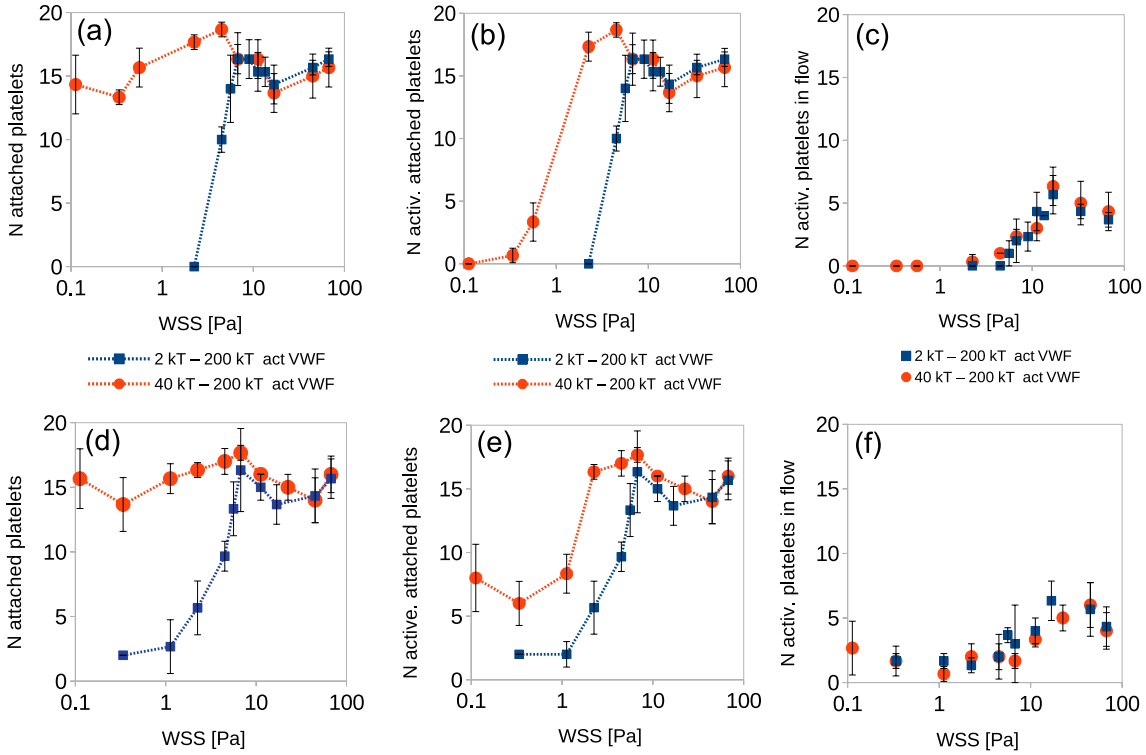

Fig. 13 The effect of mechanical $\alpha_{\mathrm{IIb}}\beta_3$ integrin activation on platelet adhesion in different hydrodynamic conditions. Panels **a-c** correspond to the conditional model (activate if $F > 10$ pN), and panels **d-f**—to the stochastic one, Eq. (15). The lines serve for visual guidance, the symbols indicate the average over at least 3 independent simulation runs, the error bars indicate the standard error. The VWF activation force was 35 pN. The GPIb-VWF binding energies were set to $A^{na}_{\mathrm{GPIb}} = 2kT$ (blue squares), $A^{na}_{\mathrm{GPIb}} = 40kT$ (red circles); $A^{\mathrm{act}}_{\mathrm{GPIb}} = 200kT$, $A_{\mathrm{int}} = 2A^{\mathrm{act}}_{\mathrm{GPIb}}$, and $A^{\mathrm{self}}_{\mathrm{int}} = 0$ for all runs. The panels (a,d) depict the number of attached platelets vs. WSS; **b,e**—the number of attached and activated platelets (with adhesive $\alpha_{\mathrm{IIb}}\beta_3$ integrins); **c,f**— the number of activated platelets flowing with the fluid (not attached to the wall). Here

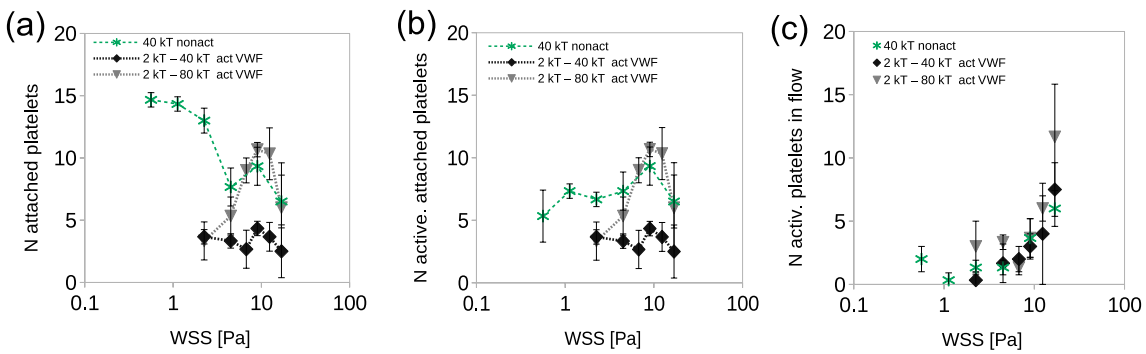

Fig. 14 Effect of abnormal GPIb-VWF binding on platelet mechanical activation and adhesion to the grafted VWF multimers in different hydrodynamic conditions. **a** The number of attached platelets versus wall shear stress. **b** The number of attached and activated platelets. **c** The number of activated platelets flowing with the fluid. The lines serve for visual guidance, the symbols indicate the average over at least 3 independent simulation runs, the error bars indicate the standard error. The VWD type 2B was simulated by the non-activatable (always sticky) VWF with $A^{\mathrm{act}}_{\mathrm{GPIb}} = A^{na}_{\mathrm{GPIb}} = 40kT$ (green asterisks). The type 2 M VWD was modeled by decreased affinity of activated VWF to GPIb: $A^{\mathrm{act}}_{\mathrm{GPIb}} = 40kT$ (black diamonds) and $80kT$ (gray triangles) with low binding energy between inactive VWF and GPIb $A^{na}_{\mathrm{GPIb}} = 2kT$. Here $A_{\mathrm{int}} = 2A^{\mathrm{act}}_{\mathrm{GPIb}}$, and $A^{\mathrm{self}}_{\mathrm{int}} = 0$ for all simulations

adhering to VWF under shear by Kuwahara et al. (1999); Nesbitt et al. (2003).

Our results are also consistent with recent findings of Liu et al. (2022) that VWF-dependent shear-induced platelet aggregation (SIPA) takes place independently from platelet activation within initial tens of microseconds, however, we also show that GPIb-mediated mechanotransduction is also possible under elevated shear stress. Present findings hint that mechanical outside-in signaling may be faster than the biochemical pathway of platelet activation, as the former may be triggered during initial 100 ms after the contact between a platelet and wall-grafted VWF multimers. This agrees with the estimation of Born and Richardson (1980); Richardson (1973). For comparison, ADP-, thrombin- or collagen-induced activation of platelets takes tens of seconds, as it follows from the typical time of classical aggregometry experiments by Packham and Rand (2011); Würtz et al. (2013) and observations of cytosolic calcium spikes by Obydennyy et al. (2016); Poole and Watson (1995); Chow et al. (1992). It also relies on diffusion of soluble agonists—a mechanism, which may become unreliable in intensive bloodstream. The time seems crucial if the near-wall shear rate is $\geq 1000\ s^{-1}$, and thus biomechanical activation appears to be a quicker and a more secure way to transduce a signal into biological response from the platelets. Also, the present study suggests that thrombus growth under high WSS triggers the mechanical activation of $\alpha_{\mathrm{IIb}}\beta_3$ integrins, which mechanically support GPIb-VWF bonds. However, GPIb-VWF plays a more important role for SIPA, since inhibition of the adhesive function of GPIb causes complete vanishing of platelet aggregation and activation in the model, while blocking of $\alpha_{\mathrm{IIb}}\beta_3$ diminished the number of stably adherent platelets at WSS$\geq$ 10 Pa, yet had no significant effect on initial recruitment. This qualitatively agrees with experimental results of Nesbitt et al. (2009).

According to these findings, we may refine our representation of the role of GPIb receptors in primary hemostasis. Under high WSS the main objective of GPIb is not only holding the platelets together, but rather probing vessel walls for active VWF multimers and triggering the activation of platelets in sites of injury or inflammation. Such *"cascade"* pattern of activation of platelet functions, probably, serves to prevent platelets from immediate aggregation and activation upon collision in the bloodstream. Another point is that the first layers of platelets recruited from the bloodstream on VWF secreted by endothelium lack sources of ADP, and therefore require alternative ways of signaling to trigger $\alpha_{\mathrm{IIb}}\beta_3$ activation and granular secretion to promote further thrombus growth.

The VWF protein itself is known to be a sensor of extreme hemodynamic conditions, e.g., in stenosed vessels, abrupt vessel cross-section changes or under elevated wall shear stress caused by arterial hypertension (Springer (2014); Nesbitt et al. (2009)). It also serves as an indicator of vascular inflammation, as endothelial cells may secrete ultra-long VWF multimers directly into bloodstream through the exocytosis of Weibel–Palade bodies (Yau et al. (2015)). But it is not enough to simply activate VWF by force—it is also required that platelets bind to it strongly and the receptor-ligand bonds withstand hydrodynamic drag for a prolonged time. Thus, together GPIb and VWF appear to be a natural biosensor system aimed at recognition of injuries or inflammation sites on vessel walls, fast harvesting of the initial information about severity of the damage (i.e., how many stretched VWF are present, how strong is the drag force, etc.), and delivering this information into a platelet via mechanotransduction pathway for further processing and fast decision making about triggering of the integrins $\alpha_{\mathrm{IIb}}\beta_3$. The latter processes rely on complex biochemical cascades of protein reactions that take place inside the cell, however, the initial steps are inherently biomechanical and mechanochemical.

The rolling dynamics of platelets is observed at the timescale of tens of seconds (up to minutes), which is much longer than the simulated 100 ms of physical time. The lifetimes of individual VWF-GPIb bonds was experimentally estimated to be in range 0.5–10 s in a range of the stretching forces 0–20 pN (Kim et al. (2010)), which is greater than the simulated physical time in the present work. Such dynamics also requires more spacious substrate areas and is normally observed in flow chambers under low and moderate shear stress (0.5−1.5 Pa), e.g. Doggett et al. (2002). Such motion pattern is related to thermal stability of the protein-protein bonds under the tension force and requires an implementation of an additional mechanism for bond rupture in the model. We may hypothesize that the rolling takes place over the inactive VWF (that is less adhesive), as the effective bond potential is rather shallow and thermal fluctuation at the molecular level may lead to bond rupture. It is possible to do in principle by using the probabilistic Monte–Carlo-like approach. However, in this particular study we focus on the initial 100 ms of the platelet attachment process and leave the long-term rolling dynamics out of the scope of the present paper. In order not to blur the model dynamics by the imposed stochastic processes, we decided to concentrate on the deterministic description in the present study. We would like to notice that in the experimental studies by Maxwell et al. (2007) of VWF-mediated platelet aggregation under the relatively high shear stress the adhering platelets remain on the position of their initial binding for several seconds. Therefore, the results of our simulations seem relevant within the mentioned limitations. Another notion here is that before the stoppage each platelet may rotate, pivot and slide on the timescale of its rotational motion in the sheared fluid ($t \approx 1/\dot{\gamma}$), i.e., several milliseconds for the shear rate of 1000/s. This dynamics is resolved by our simulations

(see Supplementary Video) and some prior works (Belyaev (2018)), yet it is difficult to grasp such fast-term motions in the experiments.

The design of the study assumed that the platelets were placed at a certain distance from the wall (equal for all platelets) and had equal chances to adhere to VWF multimers. It was chosen so in order to simplify the analysis of the results. Indeed, during the simulations the platelets may migrate from the wall due to hydrodynamic lift if they encounter no VWFs on their path or if the adhesion strength is not enough to balance the drag. However, this lift effect appears to be rather weak, as it is only noticeable at long simulation times or high shear rates. In the presented simulations, all platelets had several chances to bind to VWF, as they passed the simulated injury several (5–10) times before a significant lift from the wall was observable. However, it was noticed from visualizations of the simulations that when a free platelet collides to an attached one without establishing bonds, it may receive a boost away from the surface. This effect is physically relevant, and we did not intervene the simulations when that happened. In realistic conditions, the platelets also have a limited time to bind to the injured/inflamed patch of a vessel wall (or a flow chamber), this time decreases with increasing shear rates and platelet velocities. In the whole blood, the collisions between the RBCs and the platelets are also known to contribute to the hemostasis by pushing the platelets to the vessel wall (Bessonov et al. (2014); Tokarev et al. (2011); Spann et al. (2016)). The effect of these collisions on the integrin activation should be studied in future.

Several important issues remain out of the scope of the present study. The effect of RBCs was not studied here on purpose, as we believe that this question requires a separate systematic consideration. In order not to blur the dynamics of platelet binding to VWF by collisions with RBCs, in our simulations we decided to omit additional complexity. In contrast, here we focus on the case of platelet-rich plasma (PRP), which is a common experimental setup for in vitro thrombosis models (Zhou and Schmaier (2005)). The allosteric transitions in GPIb-VWF complex under tension resulting in catch-bond behavior (Marshall et al. (2003); Yago et al. (2008); Zhao et al. (2022)) and its effect on long-term ($\geq$ 10 s) dynamics of adherent platelets in shear remain out of the scope of the present study and should be addressed in future. Finally, in present work we use a parallel-plane geometry of the system, similar to a typical microfluidic flow chambers or lab-on-a-chip devices for laboratory studies of platelet hemostasis (Six et al. (2017); Liu et al. (2022); Roest et al. (2011)). It seems promising to study the platelet mechanical activation in more complex flow geometries resembling in vivo blood vessel shapes, wounds and stenosed areas.

In the simulations presented herein we intentionally consider the case when the VWFs are tethered at one end. Such attachment resembles the single-multimer experiments by Fu et al. (2017). This setup is also close to the situation of exposure of VWFs from Weibel–Palade bodies upon the endothelial inflammation (Schillemans et al. (2018)). Here we focus on such situations. In the literature there is a lack of information about further formation of bonds between the activated VWFs and the substrate. Several ideas, however, suggest that multiple bonds are possible. For instance, VWFs may potentially be attached to (or tangled with) the endothelial glycocalyx (Kalagara et al. (2018)). Alternatively, if the collagen fibers are present at the channel wall (in a reasonable surface density) multiple binding points could be established, since each VWF monomer contains the A3 domain responsible for that kind of adhesion (Romijn et al. (2001)). We believe that these cases deserve a separate consideration and should be addressed in future studies. However, the downstream fraction of each multimer seems to be the most flow-susceptible part of the molecule. As long as we addressed the effect of hemodynamic conditions on platelet adhesion and activation, it seems reasonable to consider only the case of a single tethering point for each VWF.

The number of modeled GPIb platelet receptors (about 100 per platelet) was smaller than in reality, because for the considered setup the limiting factor for the VWF-mediated platelet adhesion was the surface density of the tethered VWF multimers. Yet for the purpose of the current paper such GPIb density was enough, given that these receptors are homogeneously distributed over the surface of each platelet in the model. The reason is that each VWF-A1 domain can bind only one GPIb receptor. In our model, the distance between neighboring GPIb receptors was so that the excessive binding to the same VWF bead was excluded. Therefore, in the presented set of the simulations we considered that each modeled GPIb-bead mechanically represents one actual GPIb receptor, as we assume that a countable number bonds is capable of holding a platelet in the shear flow. Such assumption is justified by the estimations of GPIb-VWF bond rupture force found in Zhang et al. (2015); Chen et al. (2019): individual bonds can withstand a force of 40–60 pN, which is enough to hold a platelet against the physiological flow (for at least 100 ms). Most of the platelets in our simulations adhered by forming less than 10 bonds with the tethered VWF. Therefore, it was not necessary to increase the surface density of the GPIb-beads in the model. It might be the case though for a dense layer of adsorbed VWF (100–1000 monomers per μm^2). It is possible to apply a scaling for GPIb receptor parameters, yet it only seems reasonable, when the number of VWFs in the system is at least several orders greater. In that case one should scale both the adhesive potential and the stiffness of the springs that connect GPIb to their platelets. The condition for the GPIb MSD unfolding should be also rescaled, as the actual force on each receptor is distributed among many GPIb within

the corresponding membrane patch. With this approach it is more logical to use the probabilistic reaction rate-based kinetic account of the bonds, rather that the mechanistic method proposed in our paper. Both seem relevant for each situation, however, our goal was to investigate the possibility of platelets to bind to the surfaces with the relatively small count of grafted VWFs and inspect the possibility of their mechanical activation, thus the mechanistic approach was preferred. Another option here is to increase the number of GPIb-beads on each platelet's membrane, which will be more computationally expensive.

5 Conclusion

In the present study we implement and use coarse-grained computer simulations for accessing the dynamics of the initial stages of platelet adhesion and aggregation on wall-grafted von Willebrand factor multimers. The system was subjected to the pressure-driven flow of a viscous Newtonian fluid and various hydrodynamic conditions were simulated. The results show that platelets are likely to get activated under high shear by the interaction with surface-grafted VWF without need of any soluble agonists of platelet activation. The outcome of our analysis may allow for better understanding of complex mechanochemical phenomena that take place during initial stages of microvascular platelet-dependent thrombosis and hemostasis. Hopefully, theoretical results and methods presented in this paper would supplement the analysis of experimental studies of arterial and microvascular thrombosis, and broaden our understanding of biomechanical processes that stand behind the complex patterns of behavior and response of the living matter.

Derivation of analytical formula for estimation of the number of adherent platelets

A kinetic equation describing the adhesion of platelets in the simplest way may be formulated as follows:

$$\frac{\mathrm{d}N(t)}{\mathrm{d}t} = k_{\mathrm{on}} \cdot \left[N_0 - N(t)\right] \cdot M_{\mathrm{VWF}} - k_{\mathrm{off}}(\mathrm{WSS}) \cdot N(t), \quad (16)$$

where N_0 is the number of platelets that are located at the appropriate distance from the wall in order to participate in adhesion, M_{VWF} is the number of available adhesive VWF monomers, k_{on} and k_{off} are kinetic rates of platelet recruitment and detachment, respectively. The value of k_{on} depends on the frequency of collisions between a platelet and a VWF monomer and probability that an adhesive bond forms in the event of such collision. In our modeled case, when RBCs are absent and all identical platelets are placed at the same position from the wall, this value may be approximately considered as constant. The off-rate $k_{\mathrm{off}}(\mathrm{WSS})$ in turn is altered by the mechanical force that stretches the adhesive bonds, and thus depends on the wall shear stress (WSS). Assuming Bell-Evans kinetics, Bell (1978); Evans (1997), one may imply that:

$$k_{\mathrm{off}}(\mathrm{WSS}) = k^0_{\mathrm{off}} \cdot \exp(\alpha \cdot \mathrm{WSS}). \quad (17)$$

Seeking for a stationary solution ($\mathrm{d}N/\mathrm{d}t \to 0$) of Eq. (16), we get the following expression for the number of adherent platelets:

$$N_{\mathrm{adh}} = \frac{k_{\mathrm{on}} N_0 M_{\mathrm{VWF}}}{k_{\mathrm{on}} M_{\mathrm{VWF}} + k^0_{\mathrm{off}} \cdot \exp(\alpha \cdot \mathrm{WSS})}, \quad (18)$$

simplifying it and renaming constants, we get Eq. (14):

$$N_{\mathrm{adh}} = \frac{N_0}{1 + K \cdot \exp(\alpha \cdot \mathrm{WSS})}. \quad (19)$$

Here α determines the compliance of the adhesive contact to external forces, thus we expect it to vary with the adhesive energy between GPIb and VWF, while the "equilibrium constant" $K = k^0_{\mathrm{off}}/(k_{\mathrm{on}} M_{\mathrm{VWF}})$ is independent of the adhesive interactions and is only determined by the balance between attempts to establish or to break a bond due to collisions and thermal fluctuations of the interacting GPIb and VWF particles, respectively. Note that N_0 may be less than the total number of platelets in the simulation box, as due to platelet-platelet collisions some of them may be pushed from the wall before establishing bonds with VWF.

The application of this formula is straightforward when all the VWF monomers are equally adhesive to platelets. However, in case of the shear-induced VWF activation (i.e., $A^{\mathrm{act}}_{\mathrm{GPIb}} \neq A^{na}_{\mathrm{GPIb}}$) one expects the adherent platelet count to depend on the fraction φ of activated VWF monomers:

$$N^{(1)}_{\mathrm{adh}} = \frac{N_0 \varphi}{1 + K \cdot \exp(\alpha_{\mathrm{act}} \cdot \mathrm{WSS})} + \frac{N_0 (1 - \varphi)}{1 + K \cdot \exp(\alpha_{\mathrm{na}} \cdot \mathrm{WSS})}, \quad (20)$$

where $\alpha_{\mathrm{na}} \neq \alpha_{\mathrm{act}}$ and φ is the function of wall shear stress (*a priori* unknown).

In case of negligible affinity between non-active VWF and GPIb (low A^{na}_{GPIb}), Eq. (20) may be simplified by neglecting the second term on the right-hand side:

$$N^{(2)}_{\mathrm{adh}} = \frac{N_0 \varphi}{1 + K \cdot \exp(\alpha_{\mathrm{act}} \cdot \mathrm{WSS})}. \quad (21)$$

Also, in this case and thus in the absence of any secondary, platelet-induced VWF activation the function $\varphi(WSS)$ could be approximated by

$$\varphi(\mathrm{WSS}) = \varphi_0 \times \max\left\{0, \quad 1 - \exp\left[\beta \cdot (\mathrm{WSS} - \mathrm{WSS}_*)\right]\right\} \tag{22}$$

with $\beta = 1/4$ and WSS_* being dependent on the critical VWF activation force F_{actVWF} and fitted to comply with the number of activated VWF monomers obtained by simulations (Fig. 6b). However, for non-negligible A^{na}_{GPIb} this formula is not applicable, and numerical interpolation of φ(WSS) directly from the simulation results was used instead.

The expression Eq. (19) seems to agree with the simulations quite well in case of the non-activatable VWF monomers (Fig. 5a). For the activatable VWF with negligible A^{na}_{GPIb} Eq. (21) gives also a reasonable estimation of platelet adhesion (Fig. 6). However, for the activatable VWFs with high A^{na}_{GPIb}, there is a discrepancy between Eq. (20) and the simulations (Fig. 5b) suggesting that a more elaborated theory is required for that case. Nonetheless, if the adhesivity of non-activated VWFs is negligible, as compared to the activatable ones, Eq. (20) results in a satisfactory agreement with simulations (Fig. 6a), and so it may be used as a first-order approximation of the number of platelets bound to the wall-grafted VWF multimers with shear-switchable adhesive properties.

Supplementary Information The online version contains supplementary material available at https://doi.org/10.1007/s10237-022-01681-3.

Acknowledgements This study was supported by the Russian Science Foundation (RSF) Grant No. 22-21-00221 (https://rscf.ru/en/project/22-21-00221/). The research was carried out using the equipment of the shared research facilities of HPC computing resources at Lomonosov Moscow State University (Sadovnichy et al. (2013); Voevodin et al. (2019)).

Author contributions AVB designed the research, developed the model, performed numerical simulations, obtained and analyzed the data for Figures 2, 3 and 5–14 and the supplementary files, prepared the figures, wrote the manuscript. YKK performed part of numerical simulations and obtained the data for Figure 4. All authors reviewed the manuscript.

Funding This study was supported by the Russian Science Foundation (RSF) Grant No. 22-21-00221 (https://rscf.ru/en/project/22-21-00221/).

Data availability Raw simulation data and materials may be obtained from the corresponding author upon a reasonable request.

Declarations

Conflict of interest We declare no conflict of interest.

Ethical approval Not applicable.

References

Adhikari R, Stratford K, Cates ME, Wagner AJ (2005) Fluctuating lattice Boltzmann. Europhys Lett 71:473–479. https://doi.org/10.1209/epl/i2004-10542-5

Ahlrichs P, Dünweg B (1999) Simulation of a single polymer chain in solution by combining lattice Boltzmann and molecular dynamics. J Chem Phys 111(17):8225–8239. https://doi.org/10.1063/1.480156

Alexander-Katz A, Netz RR (2008) Dynamics and instabilities of collapsed polymers in shear flow. Macromolecules 41(9):3363–3374. https://doi.org/10.1021/ma702331d

Andrews RK, Berndt MC, López JA (2007) The glycoprotein Ib-IX-V complex. In: Michelson AD (ed) Platelets, 2nd edn. Elsevier, Burlington, pp 145–163. https://doi.org/10.1016/b978-012369367-9/50769-2

Aponte-Santamaria C, Huck V, Posch S, Bronowska AK, Grässle S, Brehm MA, Obser T, Schneppenheim R, Hinterdorfer P, Schneider SW, Baldauf C, Gräter F (2015) Force-sensitive autoinhibition of the von Willebrand factor is mediated by interdomain interactions. Biophys J 108:2312–2321. https://doi.org/10.1016/j.bpj.2015.03.041

Arce NA, Cao W, Brown AK, Legan ER, Wilson MS, Xu E-R, Berndt MC, Emsley J, Zhang XF (2021) Li R activation of von Willebrand factor via mechanical unfolding of its discontinuous autoinhibitory module. Nat Commun 12(1):1542. https://doi.org/10.1038/s41467-021-22634-x

Arnold A, Lenz O, Kesselheim S, Weeber R, Fahrenberger F, Roehm D, Košovan P, Holm C (2013) ESPResSo 3.1: Molecular dynamics software for coarse-grained models. In: Meshfree methods for partial differential equations VI, pp. 1–23. Springer, Berlin

Bell GI (1978) Models for the specific adhesion of cells to cells. Science 200:618–627. https://doi.org/10.1126/science.347575

Belyaev AV (2017) Hydrodynamic repulsion of spheroidal microparticles from micro-rough surfaces. PLoS ONE 12(8):0183093. https://doi.org/10.1371/journal.pone.0183093

Belyaev AV (2018) Catching platelets from the bloodflow: the role of the conformation of von Willebrand factor. Mat Mod Nat Phenom 13:44. https://doi.org/10.1051/mmnp/2018043

Belyaev AV (2018) Long ligands reinforce biological adhesion under shear flow. Phys Rev E 97:042407. https://doi.org/10.1103/PhysRevE.97.042407

Belyaev AV (2019) Computer modelling of initial platelet adhesion during microvascular thrombosis. Russ J Numer Anal Math Model 34(5):241–251. https://doi.org/10.1515/rnam-2019-0020

Belyaev AV (2021) Intradimer forces and their implication for conformations of von Willebrand factor multimers. Biophys J 120(5):899–911. https://doi.org/10.1016/j.bpj.2021.01.022

Belyaev AV, Panteleev MA, Ataullakhanov FI (2015) Threshold of microvascular occlusion: injury size defines the thrombosis scenario. Biophys J 109:450–456. https://doi.org/10.1016/j.bpj.2015.06.019

Belyaev AV, Dunster JL, Gibbins JM, Panteleev MA, Volpert V (2018) Modelling thrombosis in silico: frontiers, challenges, unresolved problems and milestones. Phys Life Rev 26–27:57–95. https://doi.org/10.1016/j.plrev.2018.02.005

Bessonov N, Babushkina E, Golovashchenko SF, Tosenberger A, Ataullakhanov F, Panteleev M, Tokarev A, Volpert V (2014) Numerical modelling of cell distribution in blood flow. Math Model Nat Phenom 9(6):69–84. https://doi.org/10.1051/mmnp/20149606

Born GVR, Richardson PD (1980) Activation time of blood platelets. J Membr Biol 57(2):87–90. https://doi.org/10.1007/bf01868994

Bouchnita A, Volpert V (2019) A multiscale model of platelet-fibrin thrombus growth in the flow. Comput Fluids 184:10–20. https://doi.org/10.1016/j.compfluid.2019.03.021

Bušík M, Cimrák I (2017) The calibration of fluid-object interaction in immersed boundary method. EPJ Web Conf 143:02013

Ceunynck KD, Meyer SFD, Vanhoorelbeke K (2013) Unwinding the von Willebrand factor strings puzzle. Blood 121(2):270–277. https://doi.org/10.1182/blood-2012-07-442285

Chen S, Doolen GD (1998) Lattice Boltzmann method for fluid flows. Ann Rev Fluid Mech 30:329–364. https://doi.org/10.1146/annurev.fluid.30.1.329

Chen Y, Liao J, Yuan Z, Li K, Liu B, Ju LA, Zhu C (2019) Fast force loading disrupts molecular binding stability in human and mouse cell adhesions. Mol Cell Biomech 16(3):211–223. https://doi.org/10.32604/mcb.2019.07267

Chen Y, Ju LA, Zhou F, Liao J, Xue L, Su QP, Jin D, Yuan Y, Lu H, Jackson SP, Zhu C (2019) An integrin αIIbβ3 intermediate affinity state mediates biomechanical platelet aggregation. Nat Mater 18(7):760–769. https://doi.org/10.1038/s41563-019-0323-6

Choudhary S, Sharma K, Singh PK (2021) Von Willebrand factor: a key glycoprotein involved in thrombo-inflammatory complications of COVID-19. Chem Biol Interact 348:109657. https://doi.org/10.1016/j.cbi.2021.109657

Chow T, Hellums J, Moake J, Kroll M (1992) Shear stress-induced von Willebrand factor binding to platelet glycoprotein IB initiates calcium influx associated with aggregation. Blood 80(1):113–120. https://doi.org/10.1182/blood.v80.1.113.113

Cimrák I, Gusenbauer M, Schrefl T (2012) Modelling and simulation of processes in microfluidic devices for biomedical applications. Comput Math Appl 64(3):278–288 (**Mathematical Methods and Models in Biosciences**). https://doi.org/10.1016/j.camwa.2012.01.062

Cimrák I, Gusenbauer M, Jančigová I (2014) An espresso implementation of elastic objects immersed in a fluid. Comput Phys Commun 185(3):900–907

Clemetson KJ, Clemetson JM (2014) Platelet receptors. In: Michelson AD (ed) Platelets, 2nd edn. Elsevier, Burlington

Colace TV, Diamond SL (2013) Direct observation of von Willebrand factor elongation and fiber formation on collagen during acute whole blood exposure to pathological flow. Arterioscler Thromb Vasc Biol 33(1):105–113. https://doi.org/10.1161/atvbaha.112.300522

Coller BS, Shattil SJ (2008) The GPIIb/IIIa (integrin αIIbβ3) odyssey: a technology-driven saga of a receptor with twists, turns, and even a bend. Blood 112(8):3011–3025. https://doi.org/10.1182/blood-2008-06-077891

Dayananda KM, Singh I, Mondal N, Neelamegham S (2010) von Willebrand factor self-association on platelet GpIbα under hydrodynamic shear: effect on shear-induced platelet activation. Blood 116(19):3990–3998. https://doi.org/10.1182/blood-2010-02-269266

Deng W, Xu Y, Chen W, Paul DS, Syed AK, Dragovich MA, Liang X, Zakas P, Berndt MC, Paola JD, Ware J, Lanza F, Doering CB, Bergmeier W, Zhang XF, Li R (2016) Platelet clearance via shear-induced unfolding of a membrane mechanoreceptor. Nat Commun. https://doi.org/10.1038/ncomms12863

Doggett TA, Girdhar G, Lawshé A, Schmidtke DW, Laurenzi IJ, Diamond SL, Diacovo TG (2002) Selectin-like kinetics and biomechanics promote rapid platelet adhesion in flow: the GPIbα-vWF tether bond. Biophys J 83(1):194–205. https://doi.org/10.1016/s0006-3495(02)75161-8

Dong X, Leksa NC, Chhabra ES, Arndt JW, Lu Q, Knockenhauer KE, Peters RT, Springer TA (2019) The von Willebrand factor D′D3 assembly and structural principles for factor VIII binding and concatemer biogenesis. Blood 133(14):1523–1533. https://doi.org/10.1182/blood-2018-10-876300

Dong C, Kania S, Morabito M, Zhang XF, Im W, Oztekin A, Cheng X, Webb EB (2019) A mechano-reactive coarse-grained model of the blood-clotting agent von Willebrand factor. J Chem Phys 151(12):124905. https://doi.org/10.1063/1.5117154

Dünweg B, Ladd A.J.C (2009) Lattice Boltzmann simulations of soft matter systems. In: Advanced computer simulation approaches for soft matter sciences III, pp. 89–166. Springer, Berlin

Dupin MM, Halliday I, Care CM, Alboul L, Munn LL (2007) Modeling the flow of dense suspensions of deformable particles in three dimensions. Phys Rev E 75:066707

Rusu L, Minshall RD (2018) Endothelial cell von Willebrand factor secretion in health and cardiovascular disease. In: Lenasi H (ed) Endothelial dysfunction. IntechOpen, Rijeka. https://doi.org/10.5772/intechopen.74029

Evans E, Ritchie K (1997) Dynamic strength of molecular adhesion bonds. Biophys J 72:1541–1555. https://doi.org/10.1016/S0006-3495(97)78802-7

Fedosov DA, Karniadakis GE (2009) Triple-decker: interfacing atomistic-mesoscopic-continuum flow regimes. J Comput Phys 228(4):1157–1171

Fedosov DA, Caswell B, Karniadakis GE (2010) Systematic coarse-graining of spectrin-level red blood cell models. Comput Methods Appl Mech Eng 199(29–32):1937–1948

Fedosov DA, Dao M, Karniadakis GE, Suresh S (2014) Computational bio-rheology of human blood flow in health and disease. Ann Biomed Eng 42:368–387

Fogelson AL, Hussain YH, Leiderman K (2012) Blood clot formation under flow: the importance of factor XI depends strongly on platelet count. Biophys J 102:10–18. https://doi.org/10.1016/j.bpj.2011.10.048

Fowler WE, Fretto LJ, Hamilton KK, Erickson HP, McKee PA (1985) Substructure of human von Willebrand factor. J Clin Investig 76(4):1491–1500. https://doi.org/10.1172/JCI112129

Fu H, Jiang Y, Yang D, Scheiflinger F, Wong WP, Springer TA (2017) Flow-induced elongation of von Willebrand factor precedes tension-dependent activation. Nat Commun 8:324. https://doi.org/10.1038/s41467-017-00230-2

Fukuda K, Doggett T, Laurenzi IJ, Liddington RC, Diacovo TG (2005) The snake venom protein botrocetin acts as a biological brace to promote dysfunctional platelet aggregation. Nat Struct Mol Biol 12(2):152–159. https://doi.org/10.1038/nsmb892

Furie B, Furie BC (2005) Thrombus formation in vivo. J Clin Invest 115:3355–3362. https://doi.org/10.1172/JCI26987

Furlan M (1996) Von Willebrand factor: molecular size and functional activity. Ann Hematol 72(6):341–348. https://doi.org/10.1007/s002770050184

Gardiner EE, Andrews RK (2014) Platelet receptor expression and shedding: glycoprotein Ib-IX-V and glycoprotein VI. Transfus Med Rev 28(2):56–60. https://doi.org/10.1016/j.tmrv.2014.03.001

Giupponi G, Fabritiis GD, Coveney PV (2007) Hybrid method coupling fluctuating hydrodynamics and molecular dynamics for the simulation of macromolecules. J Chem Phys 126(15):154903. https://doi.org/10.1063/1.2720385

Goto S, Salomon DR, Ikeda Y, Ruggeri ZM (1995) Characterization of the unique mechanism mediating the shear-dependent binding of soluble von Willebrand factor to platelets. J Biol Chem 270(40):23352–23361. https://doi.org/10.1074/jbc.270.40.23352

Hansen CE, Qiu Y, McCarty OJT, Lam WA (2018) Platelet mechanotransduction. Annu Rev Biomed Eng 20(1):253–275. https://doi.org/10.1146/annurev-bioeng-062117-121215

Hovinga JAK, Coppo P, Lämmle B, Moake JL, Miyata T, Vanhoorelbeke K (2017) Thrombotic thrombocytopenic purpura. Nat Rev Dis Prim. https://doi.org/10.1038/nrdp.2017.20

Jackson SP, Nesbitt WS, Westein E (2009) Dynamics of platelet thrombus formation. J Thromb Haemost 7(1):17–20. https://doi.org/10.1111/j.1538-7836.2009.03401.x

Jiang Y, Fu H, Springer TA, Wong WP (2019) Electrostatic steering enables flow-activated von Willebrand factor to bind platelet glycoprotein, revealed by single-molecule stretching and imaging. J Mol Biol 431(7):1380–1396. https://doi.org/10.1016/j.jmb.2019.02.014

Ju L, Chen Y, Xue L, Du X, Zhu C (2016) Cooperative unfolding of distinctive mechanoreceptor domains transduces force into signals. eLife. https://doi.org/10.7554/elife.15447

Kabedev A, Lobaskin V (2018) Structure and elasticity of bush and brush-like models of the endothelial glycocalyx. Sci Rep. https://doi.org/10.1038/s41598-017-18577-3

Kalagara T, Moutsis T, Yang Y, Pappelbaum KI, Farken A, Cladder-Micus L, Vidal-y-Sy S, John A, Bauer AT, Moerschbacher BM, Schneider SW (2018) Gorzelanny C The endothelial glycocalyx anchors von Willebrand factor fibers to the vascular endothelium. Blood Adv 2(18):2347–2357. https://doi.org/10.1182/bloodadvances.2017013995

Kaneva VN, Dunster JL, Volpert V, Ataullahanov F, Panteleev MA, Nechipurenko DY (2021) Modeling thrombus shell: Linking adhesion receptor properties and macroscopic dynamics. Biophys J 120(2):334–351. https://doi.org/10.1016/j.bpj.2020.10.049

Kasirer-Friede A, Cozzi MR, Mazzucato M, Marco LD, Ruggeri ZM, Shattil SJ (2004) Signaling through GP ib-IX-v activates αIIbβ3 independently of other receptors. Blood 103(9):3403–3411. https://doi.org/10.1182/blood-2003-10-3664

Kim J, Zhang C-Z, Zhang X, Springer TA (2010) A mechanically stabilized receptor-ligand flex-bond important in the vasculature. Nature 466:992–995

Konstantopoulos K, Chow T, Turner N, Hellums J, Moake J (1997) Shear stress-induced binding of von Willebrand factor to platelets. Biorheology 34(1):57–71. https://doi.org/10.1016/s0006-355x(97)00004-8

Kuijpers MJE, Gilio K, Reitsma S, Nergiz-Unal R, Prinzen L, Heeneman S, Lutgens E, van Zanvoort MAMJ, Neiswandt B, Egbrink MGAO, Heemskerk JWM (2009) Complementary roles of platelets and coagulation in thrombus formation on plaques acutely ruptured by targeted ultrasound treatment: a novel intravital model. J Thromb Haemost 7:152–161. https://doi.org/10.1111/j.1538-7836.2008.03186.x

Kulkarni S, Dopheide SM, Yap CL, Ravanat C, Freund M, Mangin P, Heel KA, Street A, Harper IS, Lanza F, Jackson SP (2000) A revised model of platelet aggregation. J Clin Investig 105(6):783–791. https://doi.org/10.1172/jci7569

Kumar RA, Dong J-f, Thaggard JA, Cruz MA, López JA, McIntire LV (2003) Kinetics of GPIbα-vWF-a1 tether bond under flow: Effect of GPIbα mutations on the association and dissociation rates. Biophys J 85(6):4099–4109. https://doi.org/10.1016/s0006-3495(03)74822-x

Kushchenko YK, Belyaev AV (2020) Effects of hydrophobicity, tethering and size on flow-induced activation of von Willebrand factor multimers. J Theor Biol 485:110050. https://doi.org/10.1016/j.jtbi.2019.110050

Kuwahara M, Sugimoto M, Tsuji S, Miyata S (1999) Yoshioka A Cytosolic calcium changes in a process of platelet adhesion and cohesion on a von Willebrand factor-coated surface under flow conditions. Blood 94(4):1149–1155. https://doi.org/10.1182/blood.v94.4.1149.416k18_1149_1155

Ladd AJC (1994) Numerical simulations of particulate suspensions via a discretized Boltzmann equation. part 2. numerical results. J Fluid Mech 271:311–339. https://doi.org/10.1017/S0022112094400178

Ladd AJC, Verberg R (2001) Lattice-Boltzmann simulations of particle-fluid suspensions. J Stat Phys 104(5/6):1191–1251. https://doi.org/10.1023/a:1010414013942

Languin-Cattoën O, Laborie E, Yurkova DO, Melchionna S, Derreumaux P, Belyaev AV, Sterpone F (2021) Exposure of von Willebrand factor cleavage site in a1a2a3-fragment under extreme hydrodynamic shear. Polymers 13(22):3912. https://doi.org/10.3390/polym13223912

Lanza F (2006) Bernard-soulier syndrome (hemorrhagiparous thrombocytic dystrophy). Orphanet J Rare Dis. https://doi.org/10.1186/1750-1172-1-46

Limbach HJ, Arnold A, Mann BA (2006) Holm C ESPResSo—an extensible simulation package for research on soft matter systems. Comput Phys Commun 174(9):704–727. https://doi.org/10.1016/j.cpc.2005.10.005

Liu ZL, Ku DN, Aidun CK (2021) Mechanobiology of shear-induced platelet aggregation leading to occlusive arterial thrombosis: a multiscale in silico analysis. J Biomech 120:110349. https://doi.org/10.1016/j.jbiomech.2021.110349

Liu ZL, Bresette C, Aidun CK, Ku DN (2022) SIPA in 10 ms: VWF tentacles agglomerate and capture platelets under high shear. Blood Adv 6(8):2453–2465. https://doi.org/10.1182/bloodadvances.2021005692

Lopez H, Lobaskin V (2015) Coarse-grained model of adsorption of blood plasma proteins onto nanoparticles. J Chem Phys 143(24):243138. https://doi.org/10.1063/1.4936908

Marshall BT, Long M, Piper JW, Yago T, McEver RP, Zhu C (2003) Direct observation of catch bonds involving cell-adhesion molecules. Nature 423(6936):190–193

Maxwell MJ, Westein E, Nesbitt WS, Giuliano S, Dopheide SM (2007) Jackson SP Identification of a 2-stage platelet aggregation process mediating shear-dependent Thrombus formation. Blood 109:566–576. https://doi.org/10.1182/blood-2006-07-028282

Mitchell WB, Li J, Murcia M, Valentin N, Newman PJ, Coller BS (2007) Mapping early conformational changes in αIIb and β3 during biogenesis reveals a potential mechanism for αIIbβ3 adopting its bent conformation. Blood 109(9):3725–3732. https://doi.org/10.1182/blood-2006-11-058420

Mody NA, King MR (2008) Platelet adhesive dynamics. part i characterization of platelet hydrodynamic collisions and wall effects. Biophys J 95:2539–2555

Mody NA, King MR (2008) Platelet adhesive dynamics. part II high shear-induced transient aggregation via GPIba-vWF-GPIba bridging. Biophys J 95:2556–2574

Mountrakis L, Lorenz E, Malaspinas O, Alowayyed S, Chopard B, Hoekstra AG (2015) Parallel performance of an IB-LBM suspension simulation framework. J Comput Sci 9:45–50. https://doi.org/10.1016/j.jocs.2015.04.006

Müller JP, Mielke S, Löf A, Obser T, Beer C, Bruetzel LK, Pippig DA, Vanderlinden W, Lipfert J, Schneppenheim R, Benoit M (2016) Force sensing by the vascular protein von Willebrand factor is tuned by a strong intermonomer interaction. Proc Natl Acad Sci 113(5):1208–1213. https://doi.org/10.1073/pnas.1516214113

Nesbitt WS, Giuliano S, Kulkarni S, Dopheide SM, Harper IS, Jackson SP (2003) Intercellular calcium communication regulates platelet aggregation and thrombus growth. J Cell Biol 160(7):1151–1161. https://doi.org/10.1083/jcb.200207119

Nesbitt WS, Westein E, Tovar-Lopez FJ, Tolouei E, Mitchell A, Fu J, Carberry J, Fouras A (2009) Jackson SP A shear gradient-dependent platelet aggregation mechanism drives Thrombus formation. Nat Med 15(6):665–673. https://doi.org/10.1038/nm.1955

Nguyen T-H, Palankar R, Bui V-C, Medvedev N, Greinacher A, Delcea M (2016) Rupture forces among human blood platelets at different degrees of activation. Sci Rep. https://doi.org/10.1038/srep25402

O'Brien JR (1990) Shear-induced platelet aggregation. The Lancet 335(8691):711–713. https://doi.org/10.1016/0140-6736(90)90815-m

Obydennyy SI, Sveshnikova AN, Ataullakhanov FI, Panteleev MA (2016) Dynamics of calcium spiking, mitochondrial collapse and phosphatidylserine exposure in platelet subpopulations during activation. J Thromb Haemost 14(9):1867–1881. https://doi.org/10.1111/jth.13395

Okhota S, Melnikov I, Avtaeva Y, Kozlov S, Gabbasov Z (2020) Shear stress-induced activation of von Willebrand factor and cardiovascular pathology. Int J Mol Sci 21(20):7804. https://doi.org/10.3390/ijms21207804

Ozaki Y, Asazuma N, Suzuki-Inoue K, Berndt MC (2005) Platelet GPIb-IX-v-dependent signaling. J Thromb Haemost 3(8):1745–1751. https://doi.org/10.1111/j.1538-7836.2005.01379.x

Packham MA, Rand ML (2011) Historical perspective on ADP-induced platelet activation. Purinergic Signall 7(3):283–292. https://doi.org/10.1007/s11302-011-9227-x

Pivkin IV, Karniadakis GE (2008) Accurate coarse-grained modeling of red blood cells. Phys Rev Lett 101(11):118105

Pivkin IV, Richardson PD, Karniadakis G (2006) Blood flow velocity effects and role of activation delay time on growth and form of platelet thrombi. Proc Nat Acad Sci 103(46):17164–17169. https://doi.org/10.1073/pnas.0608546103

Plow EF, Pesho MM (2007) Ma Y-Q Integrin αIIbβ3. In: Michelson AD (ed) Platelets, 2nd edn. Elsevier, Burlington, pp 165–178. https://doi.org/10.1016/b978-012369367-9/50770-9

Poole AW, Watson SP (1995) Regulation of cytosolic calcium by collagen in single human platelets. Br J Pharmacol 115(1):101–106. https://doi.org/10.1111/j.1476-5381.1995.tb16326.x

Pothapragada S, Zhang P, Sheriff J, Livelli M, Slepian MJ, Deng Y, Bluestein D (2015) A phenomenological particle-based platelet model for simulating filopodia formation during early activation. Int J Numer Methods Biomed Eng 31(3):02702. https://doi.org/10.1002/cnm.2702

Rack K, Huck V, Hoore M, Fedosov D, Schneider S, Gompper G (2017) Margination and stretching of von Willebrand factor in the blood stream enable adhesion. Sci Rep 7:14278

Rana A, Westein E, Niego B, Hagemeyer CE (2019) Shear-dependent platelet aggregation: mechanisms and therapeutic opportunities. Front Cardiovasc Med. https://doi.org/10.3389/fcvm.2019.00141

Reasor DA, Clausen JR, Aidun CK (2012) Coupling the lattice-Boltzmann and spectrin-link methods for the direct numerical simulation of cellular blood flow. Int J Numer Methods Fluids 68(6):767–78. https://doi.org/10.1002/fld.2534

Richardson PD (1973) Effect of blood flow velocity on growth rate of platelet thrombi. Nature 245(5420):103–104. https://doi.org/10.1038/245103a0

Roest M, Reininger A, Zwaginga JJ, King MR, Heemskerk JWM (2011) The biorheology subcommittee of the SSC of the ISTH: flow chamber-based assays to measure thrombus formation in vitro: requirements for standardization. J Thromb Haemost 9(11):2322–2324. https://doi.org/10.1111/j.1538-7836.2011.04492.x

Romijn RAP, Bouma B, Wuyster W, Gros P, Kroon J, Sixma JJ, Huizinga EG (2001) Identification of the collagen-binding site of the von Willebrand factor a3-domain. J Biol Chem 276(13):9985–9991. https://doi.org/10.1074/jbc.m006548200

Ruggeri ZM (2001) Structure of von Willebrand factor and its function in platelet adhesion and thrombus formation. Best Pract Res Clin Haematol 14(2):257–279. https://doi.org/10.1053/beha.2001.0133

Ruggeri ZM, Pareti FI, Mannucci PM, Ciavarella N, Zimmerman TS (1980) Heightened interaction between platelets and factor VIII/von Willebrand factor in a new subtype of von Willebrand's disease. N Engl J Med 302(19):1047–1051. https://doi.org/10.1056/nejm198005083021902

Ruggeri ZM, Orje JN, Habermann R, Federici AB, Reininger AJ (2006) Activation-independent platelet adhesion and aggregation under elevated shear stress. Blood 108(6):1903–1910. https://doi.org/10.1182/blood-2006-04-011551

Sadovnichy V, Tikhonravov A, Voevodin V, Opanasenko V (2013) Lomonosov: supercomputing at Moscow state university, 1st edn. Chapman and Hall/CRC Computational Science, Boca Raton

Santamaría CAA, Huck V, Posch S, Bronowska AK, Grässle S, Brehm MA, Obser T, Schneppenheim R, Hinterdorfer P, Schneider SW, Baldauf C, Gräter F (2015) Mechanosensitive von Willebrand factor protein-protein interactions regulate hemostasis. Biophys J 108(2):505. https://doi.org/10.1016/j.bpj.2014.11.2764

Savage B, Ruggeri ZM (2007) Platelet thrombus formation in flowing blood. In: Michelson AD (ed) Platelets, 2nd edn. Elsevier, Burlington, pp 359–376. https://doi.org/10.1016/b978-012369367-9/50780-1

Savage B, Saldívar E, Ruggeri ZM (1996) Initiation of platelet adhesion by arrest onto fibrinogen or translocation on von Willebrand factor. Cell 84(2):289–297. https://doi.org/10.1016/s0092-8674(00)80983-6

Schaff M, Tang C, Maurer E, Bourdon C, Receveur N, Eckly A, Hechler B, Arnold C, de Arcangelis A, Nieswandt B, Denis CV, Lefebvre O, Georges-Labouesse E, Gachet C, Lanza F, Mangin PH (2013) Integrin $\alpha_6\beta_1$ is the main receptor for vascular laminins and plays a role in platelet adhesion, activation, and arterial thrombosis. Circulation 128(5):541–552. https://doi.org/10.1161/circulationaha.112.000799

Schillemans M, Karampini E, Kat M, Bierings R (2018) Exocytosis of Weibel–Palade bodies: how to unpack a vascular emergency kit. J Thromb Haemost 17(1):6–18. https://doi.org/10.1111/jth.14322

Schneider SW, Nuschele S, Wixforth A, Gorzelanny C, Alexander-Katz A, Netz RR, Schneider MF (2007) Shear-induced unfolding triggers adhesion of von Willebrand factor fibers. Proc Nat Acad Sci 104:7899–7903. https://doi.org/10.1073/pnas.0608422104

Schwarzl R, Netz R (2018) Hydrodynamic shear effects on grafted and non-grafted collapsed polymers. Polymers 10(8):926. https://doi.org/10.3390/polym10080926

Shankaran H, Alexandridis P, Neelamegham S (2003) Aspects of hydrodynamic shear regulating shear-induced platelet activation and self-association of von Willebrand factor in suspension. Blood 101(7):2637–2645. https://doi.org/10.1182/blood-2002-05-1550

Shi X, Yang J, Huang J, Long Z, Ruan Z, Xiao B (2016) Xi X effects of different shear rates on the attachment and detachment of platelet thrombi. Mol Med Rep 13(3):2447–2456. https://doi.org/10.3892/mmr.2016.4825

Six KR, Devloo R, Aelst BV, Vandekerckhove P, Feys HB, Compernolle V (2017) A microfluidic flow chamber model for platelet transfusion and hemostasis measures platelet deposition and fibrin formation in real-time. J Vis Exp. https://doi.org/10.3791/55351

Spann AP, Campbell JE, Fitzgibbon SR, Rodriguez A, Cap AP, Blackbourne LH, Shaqfeh ESG (2016) The effect of hematocrit on platelet adhesion: experiments and simulations. Biophys J 111:577–588. https://doi.org/10.1016/j.bpj.2016.06.024

Stalker TJ, Traxler EA, Wu J, Wannemacher KM, Cermignano SL, Voronov R, Diamond SL, Brass LF (2013) Hierarchical organization in the hemostatic response and its relationship to the platelet-signaling network. Blood 121:1875–1885. https://doi.org/10.1182/blood-2012-09-457739

Sterpone F, Derreumaux P, Melchionna S (2018) Molecular mechanism of protein unfolding under shear: A lattice Boltzmann molecular dynamics study. J Phys Chem B 122(5):1573–1579. https://doi.org/10.1021/acs.jpcb.7b10796. (**PMID: 29328657**)

Succi S (2001) The lattice Boltzmann equation for fluid dynamics and beyond (numerical mathematics and scientific computation). Oxford University Press, USA

Swami A, Kaur V (2016) von Willebrand disease: a concise review and update for the practicing physician. Clin Appl Thromb Hemost 23(8):900–910. https://doi.org/10.1177/1076029616675969

Tokarev AA, Butylin AA, Ermakova EA, Shnol EE, Panasenko GP, Ataullakhanov FI (2011) Finite platelet size could be responsible for platelet margination effect. Biophys J 101:1835–1843

Tosenberger A, Ataullakhanov F, Bessonov N, Panteleev M, Tokarev A, Volpert V (2016) Modelling of platelet-fibrin clot formation in flow with a DPD-PDE method. J Math Biol 72(3):649–681. https://doi.org/10.1016/j.jtbi.2013.07.023

van Rooij BJM, Závodszky G, Azizi Tarksalooyeh VW, Hoekstra AG (2019) Identifying the start of a platelet aggregate by the shear rate and the cell-depleted layer. J R Soc Interface 16(159):20190148. https://doi.org/10.1098/rsif.2019.0148

Voevodin V, Antonov A, Nikitenko D, Shvets P, Sobolev S, Sidorov I, Stefanov K, Voevodin V, Zhumatiy S (2019) Supercomputer lomonosov-2: large scale, deep monitoring and fine analytics for the user community. Supercomput Front Innov 6(2):4–11. https://doi.org/10.14529/jsfi190201

Springer TA (2014) Von Willebrand factor, Jedi knight of the bloodstream. Blood 124(9):1412–1425. https://doi.org/10.1182/blood-2014-05-378638

Wang Y, Morabito M, Zhang XF, Webb E, Oztekin A, Cheng X (2019) Shear-induced extensional response behaviors of tethered von Willebrand factor. Biophys J 116(11):2092–2102. https://doi.org/10.1016/j.bpj.2019.04.025

Westein E, van der Meer AD, Kuijpers MJE, Frimat J-P, van den Berg A (2013) Heemskerk JWM Atherosclerotic geometries exacerbate pathological thrombus formation poststenosis in a von Willebrand factor-dependent manner. Proc Natl Acad Sci 110(4):1357–1362. https://doi.org/10.1073/pnas.1209905110

Wu W-T, Jamiolkowski MA, Wagner WR, Aubry N, Massoudi M, Antaki JF (2017) Multi-constituent simulation of thrombus deposition. Sci Rep 7:42720. https://doi.org/10.1038/srep42720

Würtz M, Hvas A-M, Christensen KH, Rubak P, Kristensen SD, Grove EL (2013) Rapid evaluation of platelet function using the multiplate® analyzer. Platelets 25(8):628–633. https://doi.org/10.3109/09537104.2013.849804

Yago T, Lou J, Wu T, Yang J, Miner JJ, Coburn L, Lopez JA, Cruz MA, Dong J-F, McIntire LV, McEver RP, Zhu C (2008) Platelet glycoprotein Ibα forms catch bonds with human WT vWF but not with type 2B von Willebrand disease vWF. J Clin Invest 118:3195–3207

Yau JW, Teoh H, Verma S (2015) Endothelial cell control of thrombosis. BMC Cardiovas Dis. https://doi.org/10.1186/s12872-015-0124-z

Yazdani A, Li H, Humphrey JD, Karniadakis GE (2017) A general shear-dependent model for thrombus formation. PLoS Comput Biol 13(1):1005291

Zhang W, Deng W, Zhou L, Xu Y, Yang W, Liang X, Wang Y, Kulman JD, Zhang XF, Li R (2015) Identification of a juxtamembrane mechanosensitive domain in the platelet mechanosensor glycoprotein ib-IX complex. Blood 125(3):562–569. https://doi.org/10.1182/blood-2014-07-589507

Zhang XF, Zhang W, Quach ME, Deng W, Li R (2019) Force-regulated refolding of the mechanosensory domain in the platelet glycoprotein ib-IX complex. Biophys J 116(10):1960–1969. https://doi.org/10.1016/j.bpj.2019.03.037

Zhao YC, Wang H, Wang Y, Lou J, Ju LA (2022) The n-terminal autoinhibitory module of the a1 domain in von Willebrand factor stabilizes the mechanosensor catch bond. RSC Chem Biol 3(6):707–720. https://doi.org/10.1039/d2cb00010e

Zhou L, Schmaier AH (2005) Platelet aggregation testing in platelet-rich plasma. Am J Clin Pathol 123(2):172–183. https://doi.org/10.1309/y9ec63rw3xg1v313